Department of Civil and Environmental Engineering

# Hydraulics of vegetated flows: estimating riparian plant drag with a view on laser scanning applications

Johanna Jalonen

Aalto University

DOCTORAL DISSERTATIONS

Aalto University publication series
**DOCTORAL DISSERTATIONS** 137/2015

# Hydraulics of vegetated flows: estimating riparian plant drag with a view on laser scanning applications

**Johanna Jalonen**

A doctoral dissertation completed for the degree of Doctor of Science (Technology) to be defended, with the permission of the Aalto University School of Engineering, at a public examination held at the lecture hall TU1 of the school on 23 October 2015 at 12.

**Aalto University**
**School of Engineering**
**Department of Civil and Environmental Engineering**
**Water and Environmental Engineering**

**Supervising professor**
Professor Harri Koivusalo

**Thesis advisor**
Dr. Juha Järvelä

**Preliminary examiners**
Professor James Brasington, Queen Mary University of London, United Kingdom
Associate Professor Maurizio Righetti, University of Trento, Italy

**Opponent**
Dr. Menno Straatsma, Utrecht University, The Netherlands

Aalto University publication series
**DOCTORAL DISSERTATIONS** 137/2015



ISBN 978-952-60-6384-3 (printed)
ISBN 978-952-60-6385-0 (pdf)
ISSN-L 1799-4934
ISSN 1799-4934 (printed)
ISSN 1799-4942 (pdf)
http://urn.fi/URN:ISBN:978-952-60-6385-0

Unigrafia Oy
Helsinki 2015

Finland

441 697
Printed matter

Aalto University

# Abstract

Aalto University, P.O. Box 11000, FI-00076 Aalto www.aalto.fi

**Author**
Johanna Jalonen

**Name of the doctoral dissertation**
Hydraulics of vegetated flows: estimating riparian plant drag with a view on laser scanning applications

**Publisher** School of Engineering

**Unit** Department of Civil and Environmental Engineering

**Series** Aalto University publication series DOCTORAL DISSERTATIONS 137/2015

**Field of research** Water and Environmental Engineering

**Manuscript submitted** 11 May 2015 **Date of the defence** 23 October 2015

**Permission to publish granted (date)** 6 August 2015 **Language** English

☐ **Monograph** ☒ **Article dissertation (summary + original articles)**

**Abstract**

In modelling vegetated flows and the associated processes, the flow resistance of riparian vegetation growing along riverbanks and floodplains has received substantial attention. This has led to the development of new resistance or drag force models and the concomitant proposal of several alternative parameters for the resistance estimation. However, the reliability of these models, the effect of reconfiguration (i.e. streamlining and bending of the specimens), and the suitability of different plant parameterizations for woody vegetation of different scales and vegetation densities have remained unclear. Moreover, retrieval of the vegetation properties is laborious with conventional methods. For data retrieval, terrestrial laser scanning (TLS) provides an advanced method which enables high-resolution surveying of floodplain topography and vegetation properties.

The aim of this dissertation was 1) to determine the main vegetation properties impacting the drag exerted by woody foliated vegetation of different scales and of varying horizontal and vertical densities, and 2) to assess the reliability of TLS as a method for obtaining herbaceous and woody vegetation properties and floodplain ground level for different seasons. For these purposes, drag force measurements were conducted in a flume in arrays and in a towing tank for natural trees of different sizes. In the flume, the plant areas of the individual specimens and the spacing of the vegetation in an array were both altered. In a towing tank, four species of 0.9-3.4 m in height were experimented together with detailed characterization of tree properties. TLS campaigns were conducted in connection with the towing tank experiments and in a field floodplain site.

The stem, leaf, and total areas proved to be reliable vegetation properties for the drag estimation despite the variability in tree height. The commonly applied frontal projected area is not an adequate parameter, as the leaves behind the frontal area still exert drag. The parameterization of the reconfiguration appeared to be independent of the tree size. Consequently, a drag force formula was derived for foliated trees with the total plant area and for the defoliated ones with the stem area as a characteristic reference area. For obtaining plant properties in the field, a new concept was proposed for reach scale analyses based on upscaling of the relationships between TLS data and manually measured plant areas derived for small sub-areas. Overall, these results of the physically-based modelling of drag forces with the TLS-based plant characterization provide useful knowledge for hydro-environmental modelling purposes.

**Keywords** vegetation, flow resistance, modelling, hydraulics, terrestrial laser scanning, remote sensing

**ISBN (printed)** 978-952-60-6384-3 **ISBN (pdf)** 978-952-60-6385-0

**ISSN-L** 1799-4934 **ISSN (printed)** 1799-4934 **ISSN (pdf)** 1799-4942

**Location of publisher** Helsinki **Location of printing** Helsinki **Year** 2015

**Pages** 132 **urn** http://urn.fi/URN:ISBN:978-952-60-6385-0

**Tekijä**
Johanna Jalonen

**Väitöskirjan nimi**
Kasvipeitteisten uomien hydrauliikka näkökulmana virtausvastuksen määrittäminen laserkeilauksen avulla

**Julkaisija** Insinööritieteiden korkeakoulu

**Yksikkö** Yhdyskunta- ja ympäristötekniikan laitos

**Sarja** Aalto University publication series DOCTORAL DISSERTATIONS 137/2015

**Tutkimusala** Vesi- ja ympäristötekniikka

**Käsikirjoituksen pvm** 11.05.2015 **Väitöspäivä** 23.10.2015

**Julkaisuluvan myöntämispäivä** 06.08.2015 **Kieli** Englanti

☐ **Monografia** ☒ **Yhdistelmäväitöskirja (yhteenveto-osa + erillisartikkelit)**

**Tiivistelmä**

Jokivarsien kasvillisuudella on merkittävä rooli tulvanhallinnassa, eroosiosuojana sekä kiintoaineen ja ravinteiden pidättäjänä. Vedenpinnankorkeuksien, virtausnopeuksien ja aineiden kulkeutumisen arvioimisen luotettavuuden parantamiseksi tarvitaan malleja, jotka käyttävät parametreina kasvien fysikaalisia ominaisuuksia ja ottavat huomioon kasvien muodonmuutoksen virtaustilanteessa (virtaviivaistuminen ja taipuminen). Puiden oksilla tehdyt kourukokeet ovat kuitenkin olleet vaikeasti skaalattavia luonnonpuille ja -pensaille. Modernit kaukokartoitusmenetelmät, kuten maalaserkeilaus (TLS), puolestaan mahdollistavat erittäin tarkan 3D-paikkatiedon keräämisen kasvillisuudesta ja sen ominaisuuksista maastossa.

Työn päämääränä oli kasvipeitteisten uomien virtausmallintamisen kehittäminen: 1) määrittämällä päätekijät, jotka vaikuttavat kasvillisuuden aiheuttamaan vastusvoimaan erikokoisilla ja erilaisilla tiheyksillä kasvavalle lehdelliselle, puuvartiselle kasvillisuudelle ja 2) selvittämällä maalaserkeilauksen luotettavuus ruoho- ja puuvartisen kasvillisuuden sekä tulvatasanteen maanpinnan kartoittamiseksi eri vuodenaikoina. Tätä tarkoitusta varten kasvillisuuden virtausvastusvoimia mitattiin laboratoriossa virtauskourussa ja hinausaltaassa. Kourussa kasvitiheyksiä vaihdeltiin sekä muuttamalla yksittäisten kasvien pinta-alaa että kasvien välisiä etäisyyksiä. Hinausaltaassa tutkittiin neljän puulajin vastusvoimia ja muodonmuutoksia virtauksessa 1-3.5 m korkeilla yksilöillä. Maalaserkeilauksia tehtiin sekä hinausallaskokeiden yhteydessä että maastossa tulvatasannealueella.

Virtausvastuksen mallinnuksessa tulisi käyttää kaavaa, jossa käytetään kokonaispinta-alaa lehdellisille puille sekä varsipinta-alaa lehdettömille puille. Kaavoissa usein käytetty kasvien projektiopinta-ala ei ole riittävä parametri, sillä lehdet projektiopinta-alan takana aiheuttivat virtausvastusta. Muodonmuutoksen vaikutus virtausvastukseen voitiin kuvata samalla parametriarvolla erikokoisille puille. Kasvillisuuden ominaisuuksien kartoittamiseksi maastossa kehitettiin menetelmä, jolla saadaan laserkeilausaineistosta virtausmallinnuksessa tarvittavat kasviparametrit eri tulvakorkeuksille ja - tarkasteluresoluutioille. Tulvatasanteen taso tulisi mitata keväällä ennen kasvipeitteen muodostumista, sillä erityisesti tiheä ruohomainen kasvillisuus estää lasersäteen pääsyn maahan asti. Maanpinnan tason määritykseen vaikuttavat mm. lasersäteen tulokulma, mittaustiheys sekä kasvillisuus ja sen tyyppi ja tiheys.

Väitöskirjan tulokset kasvillisuuden virtausvastuksen määrittämiseksi sekä lähtöaineiston keräämiseksi maastosta toimivat apuna joki- ja vesiympäristön seurannassa ja mallintamisessa.

**Avainsanat** kasvillisuus, virtausvastus, mallinnus, hydrauliikka, maalaserkeilaus, kartoitus

**ISBN (painettu)** 978-952-60-6384-3 **ISBN (pdf)** 978-952-60-6385-0

**ISSN-L** 1799-4934 **ISSN (painettu)** 1799-4934 **ISSN (pdf)** 1799-4942

**Julkaisupaikka** Helsinki **Painopaikka** Helsinki **Vuosi** 2015

**Sivumäärä** 132 **urn** http://urn.fi/URN:ISBN:978-952-60-6385-0

# Acknowledgements

The research work of this dissertation was carried out at the Aalto University, Water Engineering research group. First of all, I would like to thank the whole group for the team spirit and for creating an enjoyable work environment.

I would like to thank my instructor Dr. Juha Järvelä and my supervisor Professor Harri Koivusalo for the valuable advice they have given me along the way. Their guidance considerably helped to improve the dissertation. I am most grateful to Dr. Järvelä among many things for taking me to the research project, for the motivation and for challenging me.

For the financial support, I wish to thank the Academy of Finland, Maa- ja vesitekniikan tuki ry (MVTT), Sven Hallinin tutkimussäätiö (Sven Hallin Research Foundation) and Tekniikan edistämissäätiö (TES). The travel grants from Maa- ja vesitekniikan tuki ry have enabled my research stays in Germany and Austria, which have been essential parts of the dissertation process. I am also glad for having been able to present my work in conferences in Europe and in Central America, each important motivators for the research.

The research of this dissertation would have not been possible without collaboration with different organisations and people, both international and local. I would like to thank Professor Jochen Aberle for the research stay in the Technical University of Braunschweig, for co-authoring, and for all the help and advice I have received. Dr. Hans Peter Rauch and Clemens Weissteiner from the University of Natural Resources and Life Sciences, Vienna, are thanked for collecting the 3D EMF plant data during the towing tank experiments in Aalto. I am thankful for the research stay and warm welcome I got in Vienna and for co-authoring both conference and journal papers. My co-authors Professor Hannu Hyyppä, Juho-Pekka Virtanen, Dr. Matti Vaaja and Matti Kurkela are all thanked for their kind and perceptive commenting. I have learnt a lot from the conversations and working with them. Dr. Vahur Joala from Leica Geosystems and Jari Hotinen from Heltech are acknowledged for their collaboration. I thank my colleague Kaisa Västilä for the collaboration and friendship.

I owe thanks to Antti Louhio, technician of the water laboratory, for the help with the experiments and construction of the towing tank experimental setup. Without Antti's expertise, many of the experiments would have not been possible. I thank also laboratory technicians Aino Peltola and Marina Sushko for their assistance. I wish to thank Professor Jerzy Matusiak for allowing us to conduct the experiments in the Ship laboratory of Aalto University, and the staff of the Ship laboratory for all the help.

I express my gratitude to the pre-examiners Professor James Brasington and Associate Professor Maurizio Righetti for reviewing and for providing valuable comments on the manuscript, and to Dr. Menno Straatsma for accepting the invitation to act as my opponent in the doctoral defence.

I am grateful to the colleagues at Water Engineering for the company, for all the laughter and conversations at the coffee breaks, and for organizing various get togethers and parties, among others: Dr. Lassi Warsta, Dr. Hanne Laine-Kaulio, Gerald Krebs, Tero Niemi, Mika Turunen, Mirja Kattelus, Katri Siimes, Dr. Aura Salmivaara, Pirjo Rantanen, Leena Stenberg, Kersti Haahti, Heidi Salo, Jyrki Nurminen, Prof. Riku Vahala, Assistant Prof. Matti Kummu, Dr. Marko Keskinen, Ari Järvinen and Matti Keto. I have shared the office space with Tero, and have truly appreciated the focused but relaxed work atmosphere at the office. I am also grateful to Emeritus Professor Pertti Vakkilainen for the motivational lectures of Water resources management, which reinforced my choice to start studies in this field.

During the dissertation process I have been able to travel and meet wonderful people, and most of all, I have learnt a lot. I am thankful to my family and friends for their support and encouragement during my years in Aalto. The skiing trips and other activities, girls' cottage weekends (thank you Mia, Maria and Annika!), annual Christmas parties and other distractions my friends have arranged have all been a well needed balance for my life. Warm thanks belong to Sampsa who is entitled to a reward on understanding and flexibility as well as on listening to all my worries.

Helsinki, September 2015

Johanna Maria Jalonen

# Contents

# List of Publications

This doctoral dissertation consists of a summary and of the following publications which are referred to in the text by their numerals

**I.** Jalonen, J., Järvelä, J., Aberle, J. 2013. Leaf area index as vegetation density measure for hydraulic analyses. Journal of Hydraulic Engineering, 139(5), 461-469.

**II.** Jalonen, J., Järvelä, J. 2014. Estimation of drag forces caused by natural woody vegetation of different scales. Journal of Hydrodynamics, 26(4), 608-623.

**III.** Jalonen, J., Järvelä, J., Koivusalo, H., Hyyppä, H. 2014. Deriving floodplain topography and vegetation characteristics for hydraulic engineering applications by means of terrestrial laser scanning. Journal of hydraulic engineering, 140(11), 04014056.

**IV.** Jalonen, J., Järvelä, J., Virtanen, J.-P., Vaaja, M., Kurkela, M., Hyyppä, H. 2015. Determining characteristic vegetation areas by terrestrial laser scanning for floodplain flow modeling. Water, 7(2), 420-437.

# Author's Contribution

**Publication 1:** The author was the lead author, carried out the drag force measurements and the data analyses. The original idea of the article was grounded on the previous research of Dr. Järvelä and Prof. Aberle, and all co-authors further developed the idea of the measurements, design in the article, and participated in writing the article. The flume measurement system was designed by Prof. Aberle.

**Publication 2:** The author was mainly responsible for the design of the article, carried out the data analyses, and was mainly responsible for the writing of the article. Both co-authors were responsible for the design of the measurements. Dr. Järvelä participated in the writing of the article. Dr. Järvelä was responsible for the first idea of conducting the towing tank measurements and contributed to the organization of the measurements in the Ship laboratory of Aalto University.

**Publication 3:** The author was mainly responsible for the idea and for the writing of the article. The author carried out the data analyses. The author was mainly responsible for the design and execution of the TLS campaigns with the guidance of Dr. Järvelä. Prof. Hyyppä provided insight and guidance on the LS methodology used. All co-authors commented the manuscript, and participated in the writing of the article.

**Publication 4:** The author was fully responsible for the idea of the article and carried out the data analyses. The author was mainly responsible for the writing of the article, with commenting and suggestions on improving the manuscript by Dr. Järvelä. All co-authors commented the manuscript, took part in the writing process, and were involved in designing the investigations. The author, Mr. Virtanen, Dr. Vaaja and Mr. Kurkela conducted the field TLS campaign; the author performed the laboratory TLS; Dr. Vaaja registered the field point clouds; and Prof. Hyyppä provided insight and guidance on the LS methodology used.

# List of Abbreviations and Symbols

| | |
|---|---|
| $A_B$ | unit ground area (m²) |
| $A_C$ | characteristic reference area (m²) |
| $A_L$ | one-sided leaf area (m²) |
| $A_L/A_S$ | leaf area to stem area ratio (-) |
| ALS | airborne laser scanning |
| $A_P$ | frontal projected area (m²) |
| $A_{PW}$ | frontal projected area under water (m²) |
| $A_{PW}/A_{PW,0}$ | relative foliated frontal projected area under water (-) |
| $A_S$ | one-sided stem area (m²) |
| $A_{tot}$ | total one-sided area (m²) |
| $A_z$ | cumulative plant area at $h_z$ (m²) |
| $\chi$ | reconfiguration parameter corresponding to Vogel exponent (-) |
| $D_b$ | basal diameter (m) |
| $C_D$ | drag coefficient corresponding to $C_{D\chi}/u_\chi^\chi$ $(\mathrm{m/s})^{-\chi}$ |
| $C_{DF}$ | foliage drag coefficient corresponding to $C_{D\chi,F}/u_{\chi,F}^\chi$ $(\mathrm{m/s})^{-\chi_F}$ |
| $C_{DS}$ | stem drag coefficient corresponding to $C_{D\chi,S}/u_{\chi,S}^\chi$ $(\mathrm{m/s})^{-\chi_S}$ |
| $C_{D\chi}$ | species-specific drag coefficient (-) |
| $C_{D\chi,F}$ | species-specific foliage drag coefficient (-) |
| $C_{D\chi,S}$ | species-specific stem drag coefficient (-) |
| $c_v$ | coefficient of variation |
| DSM | digital surface model |
| DTM | digital terrain model |
| $EI$ | flexural rigidity of the main stem (Nm²) |

| | |
|---|---|
| $F_D$ | drag force (N) |
| $F_F$ | foliage drag (N) |
| $F_S$ | stem drag (N) |
| $f''$ | vegetative friction factor (-) |
| $h$ | water depth (m) |
| $H_d$ | deflected height (m) |
| $H$ | height in still air (m) |
| $H_{d,S}/H_{d,S,0}$ | relative height of the defoliated specimen underwater (-) |
| $H_d/H_{d,0}$ | relative height of the foliated specimen underwater (-) |
| $H_m$ | mean height of the herbaceous vegetation (m) |
| $h_Z$ | vertical height of vegetation (m) |
| $K$ | parameter in Eq. (7) corresponding to $C_D A_P$ (m²) |
| LAI | leaf area index, $A_L/A_B$ (-) |
| MLS | mobile laser scanning |
| $m_D$ | dry mass (g) |
| $m_{L,D}$ | leaf dry mass (g) |
| $m_{L,W}$ | leaf wet mass (g) |
| $m_{S,D}$ | stem dry mass (g) |
| $m_{S,W}$ | stem wet mass (g) |
| $N_{vox}$ | count of voxels (-) |
| $\rho$ | density of water (kg/m³) |
| SLA | the leaf to dry mass ratio $A_L/m_{d,L}$ (m²/g) |
| TLS | terrestrial laser scanning |
| $u_m$ | mean velocity (m/s) |
| $u$ | towing velocity (m/s) |
| $u_C$ | characteristic approach velocity (m/s) |
| $u_\chi$ | the lowest velocity used in determining $\chi$ (m/s) |
| $u_{\chi,S}$ | the lowest velocity used in determining $\chi_S$ (m/s) |
| $u_{\chi,F}$ | the lowest velocity used in determining $\chi_F$ (m/s) |

# 1. Introduction

## 1.1 Background

Vegetation is a critical factor in determining hydraulic resistance and water levels in floodplain and over bank flows. Typically, these riparian ecosystems between low- and high-water areas grow woody trees, bushes and shrubs with high levels of plant diversity (Richardson et al. 2007). Conventionally, vegetation along riverbanks is removed during flood protection measures, as vegetation decreases the conveyance of channels and may raise water levels. The adverse impacts on the ecological and functional state of the channels caused by standard engineering practices such as excessive channel excavation, straightening of the channels or removal of vegetation have been widely acknowledged during the past decades (e.g. Saldi-Caromile et al. 2004). Riparian vegetation plays a key role in the river restoration schemes with well recognized ecological and economic benefits, such as the increase of biodiversity, improved water quality, stabilization of river banks, increase of shade for habitats (Merritt et al. 2010; Simon and Collison 2002) and development of riparian buffer zones for flood protection (Palmer et al. 2007).

Although the resistance formulas commonly used in hydraulic analyses were brought to practice in the 18th century (Rouse and Hon 1980), accurate description of hydraulic resistance still remains a challenge, particularly for vegetated flows. The Chezy coefficient was introduced to public knowledge in 1898, and was based on a simple resistance relationship for streams developed by Chezy already in the late 1700's (Rouse and Hon 1980). The Darcy-Weisbach *f* formula is based on the work of Weisbach and Darcy for pipe flows, and is later applied to open channel flows as well (Rouse and Ince 1957). The Manning's *n* was presented at its early form in 1889 and later modified to its present form (e.g. Chow 1959). The resistance is commonly estimated through calibrated values of Manning's *n* or Darcy-Weisbach *f*, or through the coefficients derived based on lookup tables from values of similar reference sites. However, the restoration and rehabilitation measures have increased the complexity of hydraulic design in comparison to non-vegetated channels with simple geometry (Helmiö 2002).

The Manning's *n* caused by vegetation was first considered similar to surface roughness, but it was later noted that the *n* in vegetated channels decreased with increasing flow velocity (Chow 1959). The method of Cowan (1956) considers the total flow resistance consisting of a product of five factors ($n_0$ the bed roughness, $n_1$ irregularity of the channel bed, $n_2$ change in shape and size of

cross-sections, $n_3$ obstructions, $n_4$ vegetation) multiplied with the resistance caused by meandering of the channel ($m_5$). Rouse (1965) separated open channel flow resistance into surface or skin friction, form drag, wave resistance from free surface distortion and resistance due to flow unsteadiness. For estimating compound roughness, Pasche and Rouvé (1985) considered the resistance with separate friction factors of the vegetated floodplain and the main channel, and developed a method to consider the momentum exchange between the boundaries. Helmiö (2004) evaluated methods adopted to determine the composite friction factors, and derived an unsteady 1D flow model for partially vegetated natural channels considering the lateral momentum transfer.

For grass-lined channels, the $n$-$VR$ method was developed to predict $n$ based on flow velocity ($V$) and hydraulic radius ($R$) (Palmer 1945). For practical applications, the $n$-$VR$ dependency should be investigated for various types of vegetation and flow conditions, but it is difficult to derive unique $n$-$VR$ relationships even for a single vegetation type (Kouwen et al. 1969; Wilson and Horritt 2002). To resolve this issue, Petryk and Bosmajian (1975) derived a relationship between Manning's $n$ and drag force based on hydraulic radius, plant projected area $A_P$ and drag coefficient $C_D$ for cylindrical elements. For a reach section, Petryk and Bosmajian (1975) defined the vegetation density as the sum of the plant frontal projected areas per unit volume.

Vegetation in flooded areas is exposed to flow-induced forces in terms of drag and lift. The form drag is taken into account with an empirical drag force approach, which is generally based on measured values of the drag coefficient for cylinders (Nepf and Ghisalberti 2008). The pattern and density of cylinder arrays are shown to affect the bulk drag coefficient, flow velocities and thus the sediment yields (Li and Shen 1973; Nepf 1999). The drag studies with rigid cylinders have led to advances in the modelling of flows within and above vegetation (Nepf 1999; Righetti and Armanini 2002; Huthoff 2007), and to improvements in modelling of the effects of cylindrical rigid or simple shaped, flexible vegetation on mean flow, sediment transport, erosion and deposition processes (Fischer-Antze et al. 2001; Stoesser et al. 2003; Nepf and Ghisalberti 2008; Luhar and Nepf 2013; Marjoribanks et al. 2014).

For complex shaped flexible woody vegetation, idealized or cylinder based simplifications are inadequate, as vegetation reconfigures in a flow situation (i.e. vegetation changes its shape due to streamlining and bending). The vegetation properties such as density and its spatial variability, seasonal changes, the ratio of foliage in comparison to the stem, rigidity and reconfiguration under flow have all significant impacts on the drag forces and flow distribution (Aberle and Järvelä 2013). In estimating drag forces and resistance coefficients, vegetation is often assumed to be linearly distributed over the height (Aberle and Järvelä 2013). In contrast to cylindrical objects, the vertical distribution of woody vegetation differs considerably from the linear (Weissteiner et al. 2013, 2015) causing the flow to accelerate in the zones of lower plant area (Jalonen et al. 2012).

Drag forces can be directly measured from the plants with high detail (e.g. Schoneboom 2011). Similarly, detailed characterization and observations of the

reconfiguration of the plants in connection with the drag force experiments are needed to improve the process-understanding. As the remote sensing of vegetation characteristics becomes more common, new advances in the physically-based modelling of vegetated flows should be more easily implemented in practice than with conventional vegetation surveying methods. Laser scanning (LS) enables the collection of detailed digital terrain models as well as high-resolution information about vegetation and its distribution. LS is widely adopted in the monitoring of built and natural environments due to its fast acquisition of high-resolution three-dimensional information about objects (Hyyppä 2011).

To bring together the ecological considerations with the requirements of flood protection schemes requires a sound understanding of the estimation of vegetative resistance. The reliable estimation of drag exerted on woody vegetation as well as high-resolution surveying of vegetation properties are vital for determining water levels in a flood situation, sediment and solute transport (Curran and Hession 2013; Shucksmith et al. 2010), changes in channel morphology (Eaton and Giles 2009; Vargas-Luna et al. 2015) and habitat quality (Gurnell et al. 2006), as well as environmental flows and flow-regimes to predict riparian habitat development (Merritt et al. 2010). This dissertation investigates the estimation of drag exerted on riparian vegetation using physically-based vegetation characteristics and the location-based characterization of vegetation in the field required for the hydraulic modelling purposes. The motivation for this dissertation was primarily the need to improve the current knowledge of the resistance and drag parameterization for woody vegetation of different sizes, and secondly to identify efficient methods for obtaining the vegetation parameters in the field.

### 1.1.1 Vegetative resistance and drag forces

The flow resistance is often expressed in terms of a resistance coefficient, such as Manning's $n$ or Darcy-Weisbach friction factor $f$, which combines all the factors causing resistance. The Manning's $n$ remains the most commonly utilized resistance formula in hydraulic engineering practice. Literature values of Manning's $n$ are not straightforwardly transferable to hydraulic models and different processes are lumped to the $n$ value between 1D and 2D models (Horritt and Bates 2002), thus altering the value between models.

The Manning's $n$ is dimensional in contrast to the Darcy-Weisbach friction factor, and thus the latter is preferred in many studies (e.g. Fathi-Maghadam and Kouwen 1997; Järvelä 2004). A simple way to estimate the vegetative resistance is to decompose the friction factor into bed friction ($f'$) and form resistance (i.e. vegetative friction) ($f''$) by linear superposition of $f = f' + f''$ (e.g. Yen 2002). The vegetative friction factor can be derived from the spatially averaged drag force $\langle F \rangle$ per unit ground area $A_B$ (e.g. Aberle and Järvelä 2013) by

$$f'' = \frac{8\langle F \rangle}{A_B \rho u_m^2} \tag{1}$$

where $u_m$ is the mean velocity and $\rho$ is the density of water.

A common approach in 2D and 3D numerical modelling representing flow through cylindrical vegetation is based on the vegetated drag force ($F_D$) introduced as a sink term in the Navier-Stokes equations or in the Reynolds Averaged Navier-Stokes (RANS) equation for turbulent flow (Fischer-Antze et al. 2001; Morvan et al. 2008). The classical drag force approach (Hoerner 1965) expresses the total drag exerted by an object as

$$F_D = \frac{1}{2}\rho C_D A_C u_C^2 \tag{2}$$

where $C_D$ denotes the drag coefficient obtained experimentally, $A_C$ is the characteristic reference area, and $u_C$ is the approach velocity. The common definition of the reference area is the frontal projected area $A_P$ of the object perpendicular to the flow. For rigid cylinders, the drag force $F_D$ is considered to be proportional to the mean velocity squared for constant water depth and drag coefficient. For flexible foliated plants, the $F_D$-$u_m$ relationship is closer to a linear than squared (Oplatka 1998; Fathi-Maghadam and Kouwen 1997; Järvelä 2004; Armanini et al. 2005; Wilson et al. 2008; Schoneboom 2011), although it is not clear how the relationship varies for different vegetation types (Folkard 2011; Dittrich et al. 2012). The stem drag coefficient depends on the stem shape (James et al. 2008), and density and pattern of the stem array (e.g. Nepf 1999; Poggi et al. 2004; Schoneboom 2011). The drag coefficient of isolated cylinders can be obtained relating $C_D$ to the stem Reynolds number $Re_S = ud/\nu$, where $d$ is the cylinder diameter and $\upsilon$ the kinematic viscosity of water (e.g. Hoerner 1965), but it is not clear which plant scale should be used to characterize flexible and foliated plants (Statzner et al. 2006) and consequently $Re$ cannot be used to quantify reconfiguration (Luhar and Nepf 2013).

Eq. (2) is grounded on theory and experiments on rigid objects and does not truly consider the physical characteristics and hydrodynamics of flexible plants (e.g. Fathi-Maghadam and Kouwen 1997; Folkard 2011; Järvelä 2004; Wilson et al. 2010). To endure flood events, plants reconfigure themselves by both reducing the projected area under flow, which alters the effect of the characteristic reference area $A_C$, and by streamlining (de Langre 2008). The reconfiguration results in a decrease of the plant projected area $A_P$ and the drag coefficient $C_D$ which is considered by a lumped $C_D A_P$ parameter in some studies (Armanini et al. 2005; Whittaker et al. 2013; Wilson et al. 2008). The $A_P$ parameter under flow depends on the flexural rigidity of the main stem and branches, but $A_P$ for varying flow conditions and for flexible complex shaped vegetation is difficult to estimate (Sagnes 2010; Statzner et al. 2006) or to derive functional relationships for practical applications (Dittrich et al. 2012). One way to account for the reconfiguration is the Vogel exponent (de Langre 2008), where the reference area remains unaltered.

$$F_D \propto u_m^{2+\chi} \tag{3}$$

The Vogel exponent was originally considered to reflect the variation in the drag coefficient with wind speed (Vogel 1989; Vogel 1984). For rigid objects, the$\chi \approx 0$ leading to squared $F_D$-$u_m$ relationship, and $\chi = -1$ indicates a linear

relationship between force and velocity for flexible vegetation. The Vogel exponent is identical to the reconfiguration exponent $\chi$ in Eq. (5) below, and hence, the same $\chi$ symbol is used in both equations in this dissertation.

The drag coefficient is included in friction factor based approaches of Fathi-Maghadam and Kouwen (1997), Järvelä (2004) or Västilä and Järvelä (2014). Fathi-Maghadam and Kouwen (1997) suggested a method to estimate the vegetative friction factor from the momentum absorbing area ($A$), which is related to the one-sided area of leaves and stems, divided by the bed horizontal area covered by vegetation ($A_B$) as

$$f'' = 4C_D\left(\frac{A}{A_B}\right) \tag{4}$$

Järvelä (2004) proposed an approach which quantifies the resistance from the leaf area index (one-sided leaf area per ground area LAI $= A_L/A_B$), species-specific $C_{D\chi}$, and the reconfiguration exponent $\chi$ (corresponding to the Vogel exponent). The connection between Eq. (5) below and Eq. (3) was pointed out in Aberle and Järvelä (2013). Järvelä (2004) expressed the vegetative friction factor as

$$f'' = 4C_{D\chi}\frac{A_L}{A_B}\left(\frac{u_m}{u_\chi}\right)^\chi \tag{5}$$

For emergent conditions, assuming a uniform LAI over height, the level of submergence was taken into account in Eq. (5) by $h/H$, where $h$ is water level and $H$ the plant height, thus assuming a uniform plant distribution over the height. Västilä & Järvelä (2014) concluded that the different properties and reconfiguration of the stem and leaves can be considered by separating the foliage and stem friction factors by linear superposition as $f_{tot} = f_F + f_S$. They modified Eq. (5) leading to following definition of friction factor

$$f'' = \frac{4}{A_B}\left[A_L C_{D\chi,F}\left(\frac{u_m}{u_{\chi,F}}\right)^{\chi_F} + A_L C_{D\chi,S}\left(\frac{u_m}{u_{\chi,S}}\right)^{\chi_S}\right] \tag{6}$$

The subscript $F$ in Eq. (6) denotes the foliage and subscript $S$ refers to the stem, i.e. the branches and the trunk.

The flexural rigidity has been used in several studies (e.g. Kouwen and Unny 1973; Stone et al. 2013; Whittaker et al. 2013) and it is defined by $EI$, where $E$ is the modulus of elasticity and $I$ the second moment of area. Kouwen and Unny (1973) introduced a formulation $mEI$ based on the flexural rigidity $EI$ and number of roughness elements per unit bed area $m$. Kouwen and Fathi-Moghadam (2000) derived an approach for coniferous trees based on a species-specific vegetation index accounting for the effects of shape, flexibility and LAI on the resistance. The $EI$ is a measure of stem flexibility and has been adopted to model bending of woody vegetation (e.g. Stone et al. 2013), but $EI$ is not able to describe the full reconfiguration and streamlining of the branches and leaves. Whittaker et al. (2013) developed a model based on the measurements in Xavier (2009), and included the Vogel exponent ($\chi$), the tree volume ($V$), height in still air ($H$), and flexural rigidity ($EI$) as key vegetation parameters in estimating drag force as

$$F_D = \frac{1}{2}\rho K\left(u\sqrt{\frac{\rho VH}{EI}}\right)^{\chi} u^2 \quad (7)$$

where $K$ (m²) is a coefficient that corresponds to an initial $C_D A_P$. The $K$ values for Eq.(7) can be obtained from a linear relationship between $K$ and $V$ (Whittaker et al. 2013). The model quantifies the effect of reconfiguration on the drag force through $EI$ and $\chi$.

Many of the resistance studies, which have focused on physically-based parameterization of woody and aquatic vegetation (Green 2005; Green 2006; Nikora 2010; Luhar and Nepf 2013; Whittaker et al. 2013; Västilä and Järvelä 2014), have applied area-based parameterizations such as the leaf area index (LAI) (Järvelä 2004; Katul et al. 2011), leaf and stem (including branches) areas (Västilä and Järvelä 2014), the cross-sectional blockage factor (Petryk and Bosmajian 1975; Green 2006; Luhar and Nepf 2013), or the frontal area per unit volume ($A_C/V$) (Nepf and Ghisalberti 2008). For erect reeds or tree trunks these area definitions are simple to obtain based on the stem diameter and plant height. For complex shaped woody riparian vegetation, obtaining these areal parameters over the vertical tree structure is most efficient by means of remote sensing methods.

The vegetation density has been considered to be the dominating factor contributing to the drag of foliated trees (Fathi-Maghadam and Kouwen 1997; Järvelä 2004). Flow resistance investigations (e.g., Järvelä 2004; Schoneboom 2011; Västilä et al. 2011) have concluded that LAI represents a physically based parameter that characterizes the combined effect of vegetation density and foliage on flow resistance. Katul et al. (2011) applied the leaf area index in predicting hydraulic resistance with the Saint-Venant equations and Zinke (2011) with a porous media approach. However, it is not yet fully known whether LAI is an adequate resistance parameter of vegetation density for differently distributed sparse and dense vegetation stands. As reviewed above, research has suggested several alternative parameterizations for estimating vegetative resistance, but the applicability of the parameters, and the effect of reconfiguration, for determining drag of woody vegetation of different scales and densities has remained unclear.

### 1.1.2 Surrogates and real plants in the experimentation of drag exerted on plants

The experiments on living organisms, such as plants, are often conducted with surrogates or real plant prototypes (Johnson et al. 2014) where the most common simplification of vegetation uses rigid cylindrical objects (Aberle and Järvelä 2013). The surrogates are aimed to better reflect their natural counterparts than the cylinders, and are generally designed based on their material properties, modulus of elasticity, dimensions, the bending properties compared with the real plants, or by using scaled physical surrogates of plants (Johnson et al. 2014). However, for flexible plants, the scale effects are difficult to quantify. The possible scale effects in modelling the different processes in vegetated flows may be identified with a physical model at different scales up to

near full-scale, although it is laborious to apply this method (Frostick et al. 2011).

For small plants, the utilization of real plants or real size artificial plants is relatively easy. Restricted by the size of the flume, the experiments on riparian bushes and trees are often conducted with parts of trees, twigs or small trees; the hydraulic resistance of riparian vegetation has been investigated in several flume studies with natural and artificial plants or twigs both in arrays (Freeman et al. 2000; Järvelä 2004; Schoneboom 2011; Västilä et al. 2013) and with isolated plants (Armanini et al. 2005; Wilson et al. 2008). The drag and the reconfiguration or the structural properties of trees of different sizes, which are examined in this dissertation, are less explored.

Among first studies with real trees, measurements were carried out with pine and cedar trees by Fathi-Maghadam and Kouwen (1997) and with willow specimens by Oplatka (1998), Järvelä (2002a), Armanini et al. (2005) and Wilson et al. (2006) followed by others with several different species (Wilson et al. 2008; Xavier 2009; Västilä et al. 2013; Whittaker et al. 2013). Only few of the resistance or drag force studies with real scale trees are carried out in water (Oplatka 1998; Xavier 2009), though wind tunnel experiments provide comparable knowledge for air flows (e.g. Vollsinger et al. 2005). For investigating the drag forces exerted on woody vegetation, Oplatka (1998) experimented with individual willows (*Salix viminalis* and *purpurea*) of 2-3.5 m in height and pulled the specimens in a frame through a water tank with velocities of 1-4 m/s (0.5 m/s velocity increments). Xavier (2009) investigated the drag forces in a towing tank for full scale woody vegetation ($H < 4$ m). Research with prototype scale vegetation brings the resistance studies to a more general level, and should be combined with detailed characterization of vegetation properties for the drag force investigations (Schnauder and Wilson 2009). The need for studies with real scale vegetation together with detailed plant characterization brings motivation to the research questions in this study.

### 1.1.3 Laser scanning in fluvial studies

Laser scanning, often referred to as LiDAR (Light-Detection And Ranging) provides georeferenced point cloud data from which digital terrain models (DTM), digital surface models (DSM) and 3D models of objects are derived (Hyyppä 2011). LS is employed in terrestrial (TLS), airborne (ALS) and mobile (MLS) platforms (such as on a car, boat or backpack Kukko et al. 2012). The first laser instrument was developed in 1960, and first applications of ALS were employed to measure terrain features in 1960s and 1970s (Ritchie 1996) with the term LiDAR appearing at the same time (Heritage and Large 2009). The terrestrial laser scanners have become popular and the technology has developed rapidly during the past 15 years (Heritage and Large 2009). The TLS equipments can commonly record the x,y,z positions, reflection intensity and colour from a high resolution digital camera attached to the scanner. Time-of-flight based laser scanners measure the distance of the object surface using laser pulses (Lichti et al. 2002), and the continuous wave lasers by phase difference

between the transmitted and backscattered signal from the object surface (Wehr and Lohr 1999).

Conventional ground-based monitoring of floodplain topography and vegetation characteristics is time-demanding and laborious. Remote sensing methods enable deriving floodplain hydraulic roughness and DTMs efficiently from satellites (digital and radar imagery) or from airborne platforms (LiDAR and orto-photography) (Forzieri et al. 2012; Straatsma and Baptist 2008). LS provides a means to derive high-resolution data about the spatially explicit horizontal and vertical distribution of vegetation characteristics needed for the parameterization of resistance in the flow models (Antonarakis et al. 2010; Straatsma and Baptist 2008). However, the resolution and accuracy of LS measurements depend on the scanner and its distance to the object, and the platform of the LS device.

Large areas are often surveyed with ALS or MLS whereas TLS is generally applied in small-scale analyses. ALS is commonly employed in forestry in determining forest attributes such as the leaf area index (Morsdorf et al. 2006) and in hydraulic applications for estimating floodplain roughness or vegetation height and density (Forzieri et al. 2010; Forzieri et al. 2011; Straatsma and Baptist 2008). Airborne bathymetric laser scanning with blue or green wavelength laser is implemented to scan inundated areas, but the technique does not produce reliable river bed level in shallow waters (Hohenthal et al. 2011). Although TLS is commonly applied in dry conditions, recently through-water TLS has been investigated in detecting centimetre-resolution bathymetry in clear and shallow gravel bed rivers both with TLS (Smith and Vericat 2013) and with boat-based mobile laser scanning (Vaaja et al. 2013).

TLS is advantageous in retrieving more accurate data than available from ALS, as the latter provides lower point cloud density and larger footprint caused by the flight height. TLS has been recently adopted in various high-resolution studies of fluvial geomorphology, e.g. for estimating river bed morphology, roughness, and river bank retreat with as high as grain-scale accuracy (Hodge et al. 2009; Resop and Hession 2010; Brasington et al. 2012; Brodu and Lague 2012; Resop et al. 2012). The point cloud acquisition of TLS follows a spherical geometry, as it is performed from a static platform commonly mounted on a tripod, and the final resolution depends on the scanner and its distance to the object. Consequently, to reduce occlusion and to cover larger areas, TLS point clouds are produced from multiple sub-scans. MLS provides a more uniform point cloud density and decreases the measurement time in comparison to TLS, although may result to a lower point cloud density and precision (Kukko et al. 2012). MLS installed on a boat or on a backpack allows for surveying remote riverine areas (Kukko et al. 2012).

In using LS to derive floodplain topography and the vegetation characteristics, the first step is to separate the vegetation from the ground points. Although LS applications consider low vegetation generally as a factor to be extracted from the point cloud in order to obtain the ground level, hydraulic analyses require both information about floodplain topography and vegetation. In densely vegetated areas only few points return from the ground, but the ground level

may be obtained with minimum TLS elevation methods (Guarnieri et al. 2009) often employed for ALS. Furthermore, the minimum elevations together with elevation statistics help monitor river bed morphology (Brasington et al. 2012; Rychkov et al. 2012). For detecting 3D river features, such as boulders and vegetation, geometry-based classification can be applied (Brodu and Lague 2012). The large quantity of points complicates the TLS data analyses, and regular GIS software is rarely capable of processing the large TLS point clouds. To overcome this problem, TLS data can be reduced by extracting point cloud statistics and by downscaling of the information to suitable attributes such as standard deviation or the minimum and maximum elevations (Brasington et al. 2012; Rychkov et al. 2012). For TLS-based estimation of floodplain topography in vegetated areas with low bushy and herbaceous type of vegetation, the suitable scan resolution, point cloud density and the effect of different vegetation types and densities as well as seasonal change on the ground-level estimate has not been evaluated.

Laser scanning (LS) provides a means to derive the spatially explicit horizontal and vertical distribution of vegetation characteristics applied in the flow models (Antonarakis et al. 2010; Straatsma et al. 2008). For the estimation of vegetation characteristics, the vegetation density of defoliated trees is estimated with TLS from the number of points passing through a 3D voxel and from the points intercepted in the voxel (Manners et al. 2013; Straatsma et al. 2008). Leaf area can be analysed with different methods from voxelized point clouds (Béland et al. 2014; Hosoi and Omasa 2006), and the vertical leaf area distribution by the optical laser point-quadrate method (Radtke and Bolstad 2001) and by the gap fraction and the Beer-Lambert law (Antonarakis et al. 2010). The 3D LS point clouds allow for estimating the total vegetation area in contrast to photographic analyses, which estimate the frontal projected area. Moreover, photographic analyses overestimate the portion of vegetation closer to the camera due to the central projection on the image (Sagnes 2010; Straatsma and Baptist 2008).

The TLS -based methods of estimating vegetation density or leaf area are mostly developed for trees and are based on determining the vegetation density in a specific direction, i.e. the scanning direction around each scan station. Methods should be further explored for estimating total plant area from registered multi-station TLS point clouds for a varying bushy and herbaceous type of vegetation. Moreover, TLS data can be supplemented with measurements conducted from different platforms and by combining them with multi-station TLS (Manners et al. 2013; Rönnholm et al. 2009; Forzieri et al. 2011; Forzieri et al. 2012; Kukko et al. 2012) or with point clouds obtained from series of overlapping images by employing structure from motion photography (Westoby et al. 2012). Most effectively, the data analysing methods for retrieving vegetation properties should be suited for georeferenced multi-station point clouds, as well as for point clouds obtained with different platforms or remote sensing methods. To enhance the practical use of LS in hydraulic engineering applications, the need for developing such methods is a motivation for the current research.

## 1.2 Objectives and scope of the thesis

This dissertation focuses on the parameterization of riparian vegetation and on the retrieval of the vegetation properties by TLS for hydro-environmental modelling purposes. The first objective is to detect the main vegetation characteristics affecting the hydraulic drag with the focus on woody vegetation of different scales and densities, and to improve the parameterization of vegetation in the hydraulic models. The second objective is to investigate the estimation of the characteristic reference areas for mixed floodplain vegetation from multi-station TLS for both woody and herbaceous vegetation.

Recently, the modelling of the flow resistance caused by woody foliated vegetation has reached substantial attention, which has led to new flow resistance equations (e.g. Järvelä 2004; Whittaker et al. 2013; Västilä and Järvelä 2014). Subsequently, several alternative parameters for the resistance estimation are proposed. However, it is not fully known whether the resistance formulas and the proposed parameters are applicable for plants of different scales and densities. TLS enables the collection of high-resolution topographic and vegetation data required in the flow models. Many of the studies applying TLS for the characterization of floodplain vegetation focus on woody vegetation, and the estimation of the properties of varying bushy and grassy types of vegetation are less explored. LS analyses generally focus on removal of points from low vegetation, as it complicates the ground detection, but for hydraulic applications obtaining detailed information about such vegetation and its distribution is important. It is evident from the above (Section 1.1.3) that for determining physically-based and spatially accurate vegetation characteristics for hydro-environmental modelling applications, methods are required for analysing registered multi-station or multi-platform point clouds.

The publications form two pairs where I and II focus on the parameterization of riparian vegetation for the estimation of vegetative drag. The publications III and IV focus on the applicability of terrestrial laser scanning (TLS) for determining floodplain topography and the vegetation properties.

Two key questions concerning the estimation of drag forces of vegetated rivers and floodplains are addressed in the study:

A) How to reliably estimate the drag of woody riparian vegetation of different scales and vegetation densities? (Publications I and II)
B) How to obtain the location-based vegetation characteristics efficiently in the field? (Publications III and IV)

An individual leaf has different resistance characteristics than leaves attached to the plants. Similarly, individual plants affect the flow differently than a patch of plants or plants in a fully vegetated reach. For vegetation aligned in groups of plants, the sheltering effect may reduce the resistance of individual plants. The following objectives arise:

*A.1) to determine the impact of foliage and its horizontal and vertical distribution on the vegetative drag* (Publication I)

*A.2) to determine the effect of scale on the parameterization of woody riparian vegetation in modelling drag* (Publication II)

For high-resolution hydraulic modelling applications, the spatial vegetation characteristics need to be known accurately. 3D data of the distribution of vegetation can be obtained efficiently with laser scanning techniques. However, the extraction of the relevant data from the large data sets imposes a challenge for practical applications. In addition, the vegetation cover blocks the laser pulse and causes difficulties in estimating ground level for the digital terrain model (DTM). The following objectives arise:

*B.1) to determine how the type of vegetation including its seasonal change impact the accuracy of the TLS estimate of floodplain ground level* (Publication III)

*B.2) to develop a method to derive the total plant areas of herbaceous and foliated woody vegetation for different levels of submergence* (Publication IV)

Each of the publications I-IV utilizes a novel data set gathered for this dissertation. The dissertation brought new insight into the effect of both plant density and plant scale on the vegetative drag (Publications I and II). The drag force measurements of trees of different sizes with several alternative parameterizations and analyses of the reconfiguration under load, comprised a more extensive dataset than those found in the existing literature (Publication II). Consequently, a drag force formulation was derived, and its performance was evaluated against published parameter values (Publication II). TLS analyses were compared to manual vegetation and floodplain ground-level sampling, bringing new information to the reliability of TLS as a method to obtain the vegetation characteristics and floodplain ground level for different seasons and low floodplain vegetation of both woody and herbaceous type of vegetation (Publications III-IV).

## 1.3 Publications

Publication I investigated the impact of density and distribution of leaf area on the vegetative drag. A dataset was gathered in which the leaf area index (LAI = $A_L/A_B$) was widely varied: (1) the distances between the plants were altered, and (2) the one-sided plant areas of the individual specimens were doubled and tripled. In addition, the new dataset was compared with previous experiments in which the vertical leaf area distribution was varied.

Publication II investigated the suitable parameterization of woody riparian vegetation of different scales in estimating the drag forces. Experiments were conducted in a towing tank for four tree species together with detailed characterization of tree properties. The focus was on the effect of plant scale on the vegetative drag and reconfiguration. The suitability and reliability of different parameterizations of woody riparian vegetation for physically-based drag force models was tested.

Publication III focused on the application of TLS in determining floodplain topography and vegetation properties. The publication demonstrated 1) the impact of vegetation and its seasonal change to the accuracy of the TLS estimates of floodplain ground level, 2) the effect of point cloud density on the TLS-based ground level, and 3) the applicability of TLS to estimate vegetation height and the volumetric blockage factor for different levels of submergence. The TLS-based ground level and vegetation estimates were evaluated against manual cross-sectional and vegetation surveys.

Publication IV continued the research of Publication III for obtaining the properties of floodplain vegetation. The focus was on developing an approach for deriving the characteristic reference areas of both herbaceous and woody vegetation. Detailed experimental data was used to obtain linear regressions between TLS-based point cloud attributes and manually surveyed total plant areas for both herbaceous and woody vegetation. Finally, a novel concept was proposed to derive the total plant area ($A_{tot}$) for larger areas of similar vegetation type from linear regressions between TLS-based point cloud attributes and $A_{tot}$ of small sub-areas.

# 2. Methods

Figure 1 shows the methodology adopted in the dissertation. The main methodology is described in the following sections, and the more detailed descriptions can be found in the referred publications (I-IV).

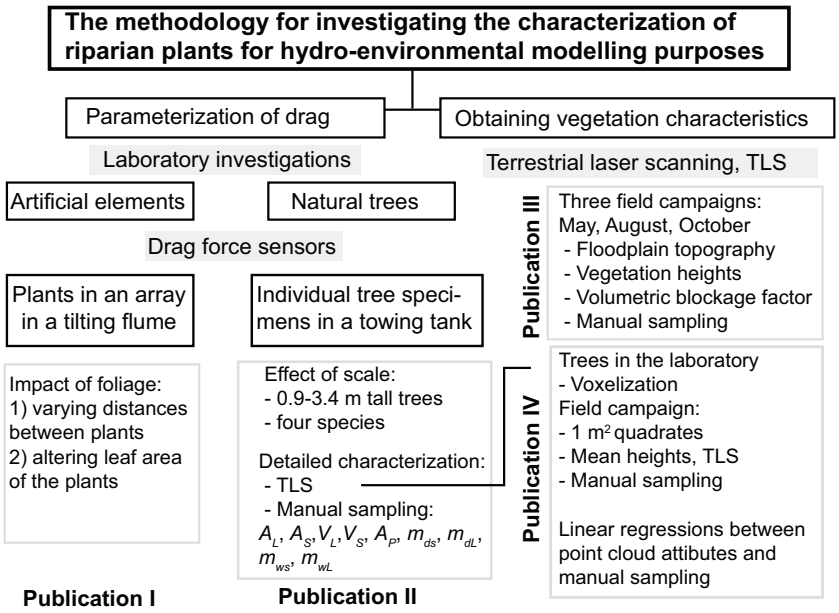


Figure 1. The methodology adopted in the dissertation to investigate the characterization of riparian plants for hydro-environmental modelling purposes.

## 2.1 Hydraulic investigations

### 2.1.1 Flume experiments

The flume experiments (Publication I) were carried out at the hydraulic laboratory of the Leichtweiß-Institute for Hydraulic Engineering and Water Resources, Technische Universität Braunschweig, Germany. The tilting flume was 32 m long, 0.6 m wide and 0.4 m deep. The study was conducted with 23 cm high foliated artificial vegetation elements simulating natural poplars. The properties of the artificial elements were found to be similar to the branches of natural poplars (Dittrich et al. 2012) by analyses of the lever arm and drag of the artificial elements compared to natural poplar twigs (Schoneboom 2011).

Artificial elements were used to ensure that the plant characteristics were similar for each specimen, thus excluding the variability in plant properties of natural poplars. The individual elements consisted of a 3 mm thick coated wire stem, four branches with three leaves each made of fully flexible dyed textile, and a rigid blossom on the top (Figure 2a). The total one-sided area of a single element ($A_{tot}$ = 393.70 cm²) corresponded to the sum of the one sided leaf area ($A_L$ = 373.6 cm²) and one-sided stem area ($A_S$, stem + blossom = 20.12 cm²). The leaf area index (LAI $= A_L/A_B$) values ranged between 0.2 and 3.2, and thus the densest setups were close to the mean values in broadleaf forests and floodplains (Publication I).

The total plant areas and the leaf areas (Publication I) were varied by changing the plant area of the individual specimens, i.e. combining the artificial plant elements (1-element plants 1X, 2-element plants 2X and 3-element plants 3X, Table 1, Figure 2a). In addition, the effect of altered vertical leaf area was investigated for the plant elements, which had the branches removed from the top (1) to the base (4) (data from Schoneboom 2011). The plants with varying vertical leaf area were labelled as 123●, 12●4, 12●● and 1●●● (Table 1, Figure 2a). The dots denote the removed branches consisting of three leaves each, and the numbers denote the branches from top (1) to base of the plant element (4). The spacing of the plants in a staggered arrangement was altered from 15 to 40 cm (Figure 2b).

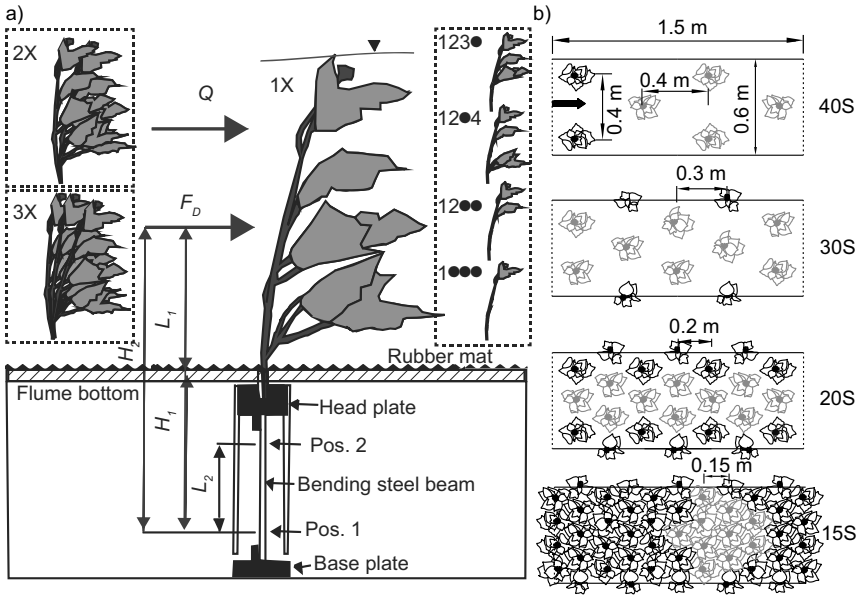


Figure 2. a) The drag force sensor and the studied plant elements: 1-element plant 1X, 2-element plant 2X and 3-element plant 3X, and plants with varying vertical leaf area distribution labelled as 123●, 12●4, 12●● and 1●●●. The dots denote the removed branches and the numbers denote the branch from top (1) to base of the plant element (4), and b) plant arrangements 15S, 20S, 30S and 40S at the test section. The lighter-coloured symbols denote the plants attached to the drag force sensors. (Publication I).

The drag forces acting on up to 10 plants (Figure 2b) were directly measured from the plants with drag force sensors (DFS, Figure 2a) mounted below the flume bottom. The plants were arranged in a staggered pattern in a 10-12.5 m long flume section, and the drag force sensors were placed in a 1.5 m long test section in the middle of the plant arrangement. The sampling rate was set to 200 Hz and the standard error corresponded to ±0.01N. The drag forces were recorded for a 60 s sampling interval. Each measurement was conducted three times, and a high degree of consistency was found between the three measurements. The total plant area per ground area ($A_{tot}/A_B$) was altered by changing $A_{tot}$ of the individual plants and by altering the plant spacing (Figure 2b, see Table 1 for the investigated setups).

The frontal projected areas ($A_P$) of the plants under flow action were estimated from photographs taken with a submersible digital camera. All of the experiments were conducted with steady uniform flow conditions, with the plants just submerged (Figure 2a), to enable analysing the effect of leaf area on the vegetative drag. The flow conditions were achieved by adjusting the water level, discharge, and bed slope. The water levels varied in the experiments due to bending of the plants (Figure 2a). The water depths, and the water surface slopes, were measured by five piezometers installed along the flume. For the setups in Table 1, flow resistance and drag forces were measured for four to seven mean flow velocities ranging between 0.11 and 0.92 m/s. The corresponding mean water depths in the test section varied from 0.26 to 0.18 m.

**Table 1.** Description of the investigated setups: spacing $a_x a_y$, number of plant elements NX, one-sided leaf area $A_L$, leaf area index LAI, total one-sided area $A_{tot} = A_L + A_S$, leaf to stem area ratio $A_L/A_S$ and number of plant elements/m². (Publication I).

| $a_x a_y$ | NX | $A_L$ (cm²) | LAI | $A_{tot}$ (cm²) | $A_L/A_S$ | Elements/m² |
|---|---|---|---|---|---|---|
| 15x15S | 1X* | 373.6 | 1.66 | 393.7 | 18.6 | 44.44 |
| | 2X | 747.2 | 3.32 | 787.4 | 18.6 | 88.89 |
| 20x20S | 1X* | 373.6 | 0.93 | 393.7 | 18.6 | 25.00 |
| | 2X | 747.2 | 1.87 | 787.4 | 18.6 | 50.00 |
| | 1X 123●* | 237.8 | 0.59 | 257.9 | 11.8 | 25.00 |
| | 1X 12●4* | 264.3 | 0.66 | 284.4 | 13.2 | 25.00 |
| | 1X 12●●* | 128.5 | 0.32 | 148.6 | 6.4 | 25.00 |
| | 1X 1●●●* | 66.0 | 0.17 | 86.14 | 3.3 | 25.00 |
| 30x30S | 1X* | 373.6 | 0.42 | 393.7 | 18.6 | 11.11 |
| | 2X | 747.2 | 0.83 | 787.4 | 18.6 | 22.22 |
| | 3X | 1120.8 | 1.25 | 1181.1 | 18.6 | 33.33 |
| 40x40S | 1X | 373.6 | 0.23 | 393.7 | 18.6 | 6.25 |
| | 2X | 747.2 | 0.47 | 787.4 | 18.6 | 12.50 |
| | 3X | 1120.8 | 0.70 | 1181.1 | 18.6 | 18.75 |

*Schoneboom (2011)

### 2.1.2 Towing tank experiments

The towing tank experiments were conducted for four tree species totalling 23 specimens of 0.9–3.4 m in length (Table 2, more detailed description in Table 1 in Publication II) in a 130 m long, 11 m wide and 5.5 m deep towing tank at the ship laboratory of the Aalto University (Publication II). The drag forces were

directly measured from the trees with a frequency of 80Hz using load cell setups consisting of three load cells (Figure 3). To allow for accurate force measurement, two different load cell types were applied depending on the size of the specimen (for large trees, 1 -1000 N measurement range and for smaller trees, 0.1 – 100 N). Each of the load cells, and the load cell combination, were calibrated and validated with known weights. The measurement error of the load cells based on the validation was ±0.1% for the large tree load cells and ±0.2% for the small tree load cells. The trees were mounted upside-down to the measurement system with an aluminium cylinder of 35 mm in diameter, and the natural curvature of the main stem was directed downstream, opposite to the towing direction.

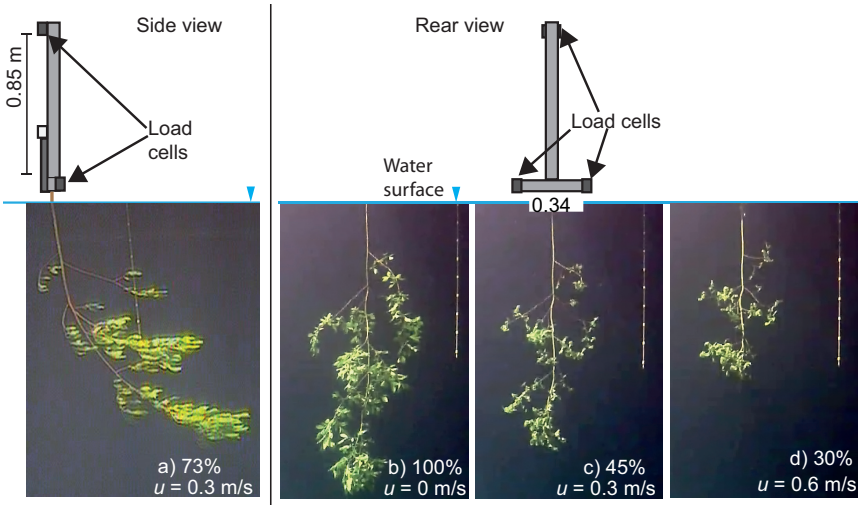


Figure 3. The drag measurement system with side and rear views (Publication II). The picture a) illustrates the specimen (SC7) from the side view camera with a velocity of 0.3 m/s and b-c) from the rear view with b) 0 m/s, c) 0.3 m/s and d) 0.6 m/s (data from Publication II). The percentages denote the percentage of height compared to zero velocity (a) and percentage in the frontal projected area in zero velocity (b-d).

The submerged side and rear view cameras were used to collect underwater video recordings. The side and rear view cameras were attached at a distance of 3 m and 5.5 m, respectively, from the specimens. The length scale for the image analysis of the underwater projected area $A_P$ was adjusted to the side of the tree (Figure 3). The measured tree height in still air was used as a length scale for analysing the deflected height of the tree. The investigated velocity ranges were 0.1-1.5 m/s for the foliated specimens and 0.1-2.5 m/s for the defoliated ones. The foliated specimens were already streamlined close to a maximum at a velocity of 1.5 m/s; hence, larger velocities would have caused breakage or changes in the material properties. The specimens were towed in one direction, and after each run the carriage was brought back to the starting position. The next run was conducted after there was no disturbance in the water caused by the previous run.

The one-sided areas of the tree stems (branches and trunk) were obtained from manual measurements assuming that the stems and branches were

cylindrical elements (see Weissteiner et al. 2013, 2015). Due to the large size of the trees, the specific leaf area (the leaf to dry mass ratio, SLA $= A_L/m_{d,L}$, Bréda 2003) was applied to estimate the total leaf area of the tree. The trees were divided to four height sections (quartiles), and the leaf and stem dry mass was estimated for each section. The leaf areas were measured from the second highest section from the top by scanning the leaves with a flatbed document scanner. To ensure the accuracy of SLA, the leaves from this second quartile were divided to three different samples, and SLA was determined for each sample. For the investigated specimens, the difference between the SLA of a sample and the average of three samples varied from 0% to 6%. The total plant area $A_{tot}$ was estimated from the manually measured $A_L$ and $A_S$.

**Table 2.** The investigated species and the range of the heights and plant areas of the specimens

| Species | Common name | No. | Heigth (m) | $A_{tot}$ ($m^2$) | $A_L$ ($m^2$) | $A_S$ ($m^2$) | $A_L/A_S$ (-) |
|---|---|---|---|---|---|---|---|
| *Alnus glutinosa* | Common Alder | 6 | 1.2 – 3.0 | 0.43 – 3.0 | 0.41 – 2.8 | 0.023 – 0.19 | 11-26 |
| *Salix caprea* | Goat Willow | 9 | 1.0 – 3.4 | 0.44 – 2.2 | 0.42 – 2.0 | 0.023 – 0.47 | 9.6-18 |
| *Betula pendula* | Silver Birch | 4 | 0.9 – 2.8 | 0.49 – 2.0 | 0.47 – 2.2 | 0.018 – 0.15 | 12-27 |
| *Betula pubescens* | White Birch | 4 | 1.5 – 3.2 | 0.44 – 1.0 | 0.42 – 0.96 | 0.025 – 0.06 | 11-17 |

### 2.1.3 Drag force equations

For this dissertation, the drag force formulations were derived based on rearranging of friction factor Eqs. (5) and (6) in terms of drag (Publication II). Based on Eq. (5), the drag coefficient for rigid cylinders $C_D$ in Eq. (2) corresponds to a dimensionless number $C_{D,\chi}u_m^{\chi}/u_{\chi}^{\chi}$ for woody flexible vegetation. However, derived from the drag force Eq. (3) including the reconfiguration exponent, the friction factor based on drag force Eq. (1) and the friction factor Eq. (5) leads to

$$\frac{8\left\langle \frac{1}{2}\rho C_D A_C u_m^{2+\chi}\right\rangle}{A_B \rho u_m^2} = 4C_{D\chi}\frac{A_L}{A_B}\left(\frac{u_m}{u_\chi}\right)^{\chi} \tag{8}$$

The Eq. (8) leads to $C_D = C_{D\chi}/u_{\chi}^{\chi}$ having units of $(m/s)^{-\chi}$ (Publication II). Combination of $C_{D\chi}/u_{\chi}^{\chi}$ should not change while the exponential relationship between force and velocity remains the same, but would simplify drag force equations (9-11) below (Publication II). If the reconfiguration exponent changes for different ranges of velocities, the $C_{D\chi}$ and the share $C_{D\chi}/u_{\chi}^{\chi}$ are both altered (Publication II). The drag force formulation based on Eq. (5) for a single tree becomes

$$F_D = \frac{1}{2}\rho\frac{C_{D\chi}}{u_{\chi}^{\chi}}A_L u_m^{2+\chi} \tag{9}$$

The stem and foliage drag based on Eq. (6) are written as

$$F_S = \frac{1}{2}\rho\frac{C_{D\chi,S}}{u_{\chi S}^{\chi S}}A_S u_m^{2+\chi S} \tag{10}$$

$$F_F = \frac{1}{2}\rho\frac{C_{D\chi,F}}{u_{\chi,F}^{\chi_F}}A_L u_m^{2+\chi_F} \tag{11}$$

The measured foliage drag was evaluated from the measured stem drag and bulk drag as $F_F = F_D - F_S$ (e.g. Armanini et al. 2005; Wilson et al. 2010; Västilä and Järvelä 2014). The level of flexibility and streamlining in Eqs. (9-10) is described by the reconfiguration parameter $\chi$. For rigid elements, the$\chi \approx 0$ resulting to the classical drag force Eq. (3), and $\chi$ close to $-1$ denotes efficient reconfiguration of the specimens.

The suitability of different plant parameterizations for physically based modelling applications, and the performance of Eqs. (7), (9) and (10) for trees of different sizes is evaluated in section 3.2.

## 2.2 Terrestrial laser scanning of vegetation properties and floodplain topography

### 2.2.1 TLS campaigns

TLS was carried out both in the laboratory for the trees in connection with the towing tank experiments (Section 2.1.2, Publication II) and in the field (Publications III and IV). Field investigations were conducted in Sipoo in Southern Finland (latitude 60.334, longitude 25.220) at a 200 m long reach of a compound, two-stage, channel with a bankful width of 11 m and floodplain width of 4-6 m (Västilä et al. 2015b). The vegetation in the five investigated 20 m long test reaches consisted of naturally established mixed grasses, two reaches of sown pasture grasses, ~1 m tall willows, and bare soil (Figure 4). The test reaches Willows-M and Bare-M were maintained free of grasses by cutting, whereas the other three reaches were left to natural succession.

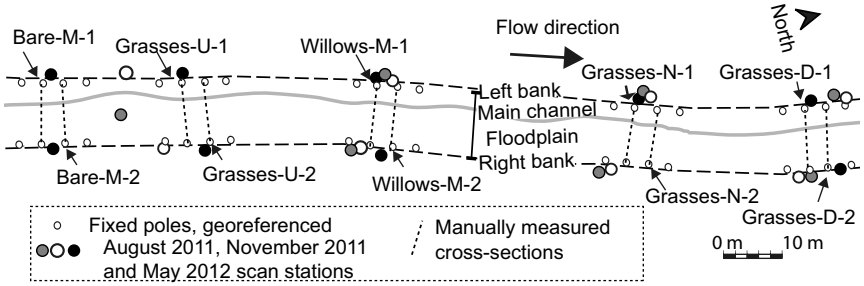


Figure 4. The TLS campaigns 2011-2012 at the field site with locations of the scan stations and cross-sections (Publication III).

Altogether four measurement campaigns were conducted at the channel (Figures 4 and 6, Table 3). Initially, the site was laser scanned in August 2011 with a pulse-based scanner Leica ScanStation 2 and in November 2011 and May 2012 with ScanStation C10 (Publication III). The ScanStations have an integrated camera, 360° × 270° field of view, a range up to 300 m, a scan rate up to 50,000 points/s, and a 4 mm spot size (at 0-50 m distance). The scan resolution was set to 2 cm at a distance of 20 m from the scanner in November 2011 and in May 2012. To estimate the impact of scan resolution on the TLS-based ground level, the August 2011 scans were partly conducted with a higher resolution of 1 cm at a distance of 20 m. To decrease occlusion, the scans were

performed from the channel banks from both sides of the channel. Spherical targets were used for the registration and georeferencing, with local coordinates surveyed with a total station (Figure 4) (averaged error of x,y,z coordinates < 5 mm).

To analyse vegetation characterization in more detail, an additional field campaign was conducted with Faro Focus 3D in August 2013 (Publication IV). Three of the test reaches were scanned from multiple locations (from both banks and the floodplain, Figure 6). The Faro laser scanner has a 305° × 306° field of view, a range up to 153 m, a scan rate up to 976,000 points/s and a beam divergence of 0.19 mrad. The scan was performed with a point spacing of 1.2 cm at a distance of 20 m. In a laboratory, TLS was conducted for six 1.8-3.4 m tall trees, with three foliated *Alnus glutinosa* and *Salix caprea* specimens (Publication IV). To ensure complete coverage, the trees were laser scanned from three directions with the Leica ScanStation C10. The scanning resolution used was 1 cm at a distance of 20 m. The individual scans were co-registered in Leica's Cyclone software using spherical targets with the co-registration error of 0-2 mm.

**Table 3.** The field TLS datasets

| Year | Month | Instrument | Publication |
|---|---|---|---|
| 2011 | August | Leica ScanStation 2 | III |
| 2011 | November | Leica ScanStation C10 | III, IV |
| 2012 | May | Leica ScanStation C10 | III, IV |
| 2013 | August | Faro Focus 3D | IV |

### 2.2.2 TLS analyses of floodplain topography

To create a digital terrain model (DTM) of the ground surface, the lowest elevations were selected from the point cloud with window sizes of 10, 30, 50 and 100 cm and a triangular irregular network (TIN) was created from each dataset (Publication III). To evaluate the optimal window size at the floodplain area, including the right bank slope, a DTM raster of 5 cm in resolution was created with the natural neighbour interpolation. These TLS analyses were compared to manual cross-sectional measurements (Västilä et al. 2015b) with horizontal distances of 0.2-0.4 m and a vertical accuracy of approximately ±6 mm. The cross-sections were located in the middle of the test reaches at 4 m distance from each other, and are referred to as cross-sections 1 and 2 for each test reach (e.g. Grasses-D-1, see Figure 4). The difference between the TLS-based DTM and the manually measured cross-sectional elevations was evaluated with the mean absolute error (MAE, Publication III).

The impact of the point cloud density on the ground detection was estimated for the Willows-M and Grasses-D by creating DTMs for the original point clouds and for the point clouds decreased to 25,11, and 6% of the original. Consequently, the error was evaluated from MAE in comparison to the manual reference measurements. Similarly, the differences in MAE of DTM for the registered point cloud in comparison to the individual point clouds from the left and right bank scan stations were evaluated for the two test reaches.

### 2.2.3 TLS analyses of vegetation properties

Manual vegetation samples were gathered from 4-6 randomly selected quadrates of 12.5 × 12.5 cm² in the test reaches Grasses-U, -N and -D for Publication III in connection with the TLS campaign of August 2011 and by Västilä et al. (2015b) during the monitoring of the field site. The dry mass and mean heights were analysed from the samples. The vertical distribution of one-sided plant area was estimated for 10 cm height increments using image analysis. A digital surface model (DSM) of the vegetation on the floodplain was obtained by selecting the highest points in 1 cm and 5 cm rasters (Figure 5). To derive vegetation heights, TLS-derived DTM was subtracted from DSM. Subsequently, the volume occupied by the vegetation was estimated for 10 cm height increments.

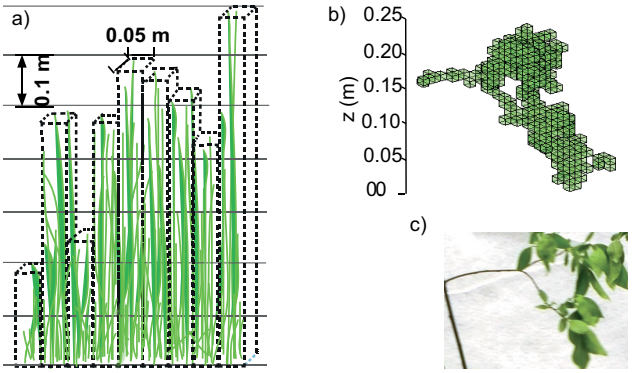


Figure 5. a) Volumetric approach to determine vegetation height and the portion of vegetation volume in 10 cm height increments (Publication III). b) A voxelized branch and c) a photograph of a branch of *S. caprea* specimen (SC3) (Publication IV).

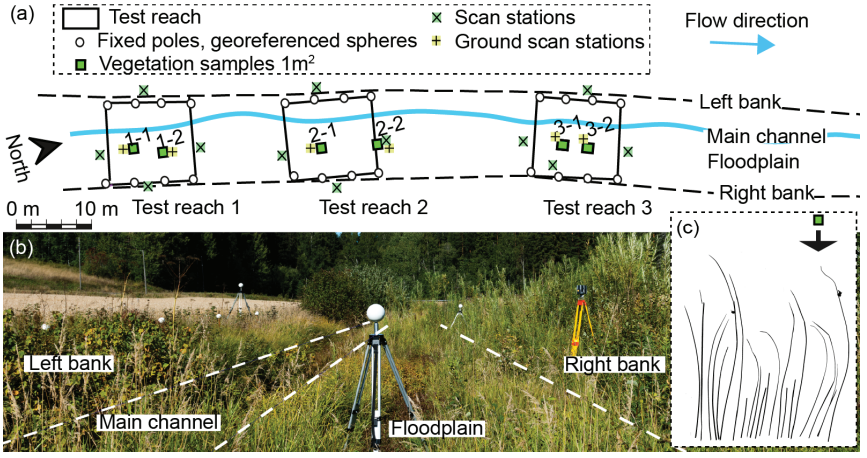


Figure 6. Field campaign 2013: a) locations of the scanner and vegetation sampling quadrates, b) the TLS campaign at the reach in dry conditions, and c) example of sampled vegetation photographed for the estimation of $A_{tot}$. (Publication IV)

For detailed analyses of vegetation characterization, all of the vegetation was gathered from two 1 m² quadrates in each of the scanned test reaches during the

August 2013 TLS campaign (Figure 6). The total plant area ($A_{tot}$) was estimated from photographs of the vegetation samples using image analysis. To obtain ground level, these quadrates were scanned after the removal of vegetation, and DTM of the sampling quadrates was obtained by selecting the lowest elevations in a 1 cm grid. For the 1 m² quadrates in the floodplain, the vegetation heights were derived in 1 cm, 5 cm and 10 cm grid resolutions.

For the TLS analyses of trees (Publication IV), the point cloud was sampled to a voxel grid (Figure 5b). Firstly the incorrect points appearing e.g. from the edges of leaves were filtered with a statistical filtering removal SOR (Rusu et al. 2008). The filtering removes the outliers, i.e. points whose mean distances are outside an interval defined by the global distances mean and standard deviation. Fifty points were used for the mean distance estimation and the standard deviation multiplier threshold used was one (Publication IV). The filtered point cloud was subsampled by a minimum distance of 1 cm between the points and sampled to $1, 5$ and 10 cm voxel grids with the centroids of the voxels recorded. A linear regression was derived between the manually sampled $A_{tot}$ and voxel count ($N_{vox}$) of the trees. The vertical distribution ($A_z$) of the total plant area of trees was estimated for eight vertical height sections by applying the linear regression.

# 3. Results

## 3.1 Parameterization of woody riparian vegetation

The flume experiments conducted by varying the leaf area of artificial poplars in an array were adopted to investigate the applicability of $A_{tot}/A_B$ and $A_L/A_B$ as vegetation density measures (Publication I). The spatially averaged drag forces as a function of mean flow velocity (Publication I) are shown in Figure 7 for all the investigated setups of Table 1, Figure 2.

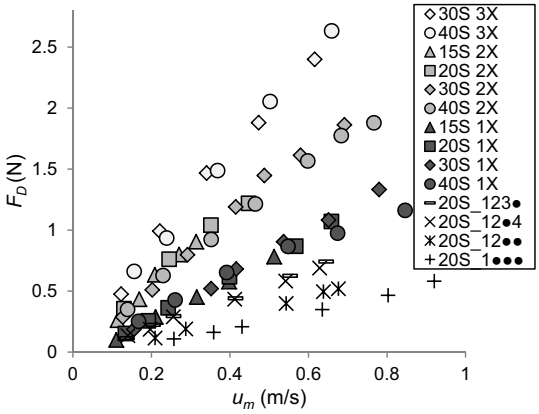


Figure 7. Spatially averaged drag forces $\langle F_D \rangle$ as a function of mean flow velocity for the different investigated setups (Table 1). 3X and 2X denote the multi-element plants and 1X denotes the one-element plants. 123●-1●●● refer to the plants with varying vertical leaf area. The dots (●) denote the removed branches, and the numbers denote the branches from top (1) to base of the plant element (4). (See Figure 2 and 3 for the plant setups). (Publication I).

The normalization of the drag forces with total plant area is depicted against velocity in Figure 8. The analyses revealed that the normalized drag forces fell close to a single curve for all the investigated setups and plant elements. $F_D/A_{tot}$ of the multi-element plants (2X and 3X) fell, however, below the one-element plants (1X), particularly for velocities larger than 0.4 m/s (Figure 8c-d). The difference between the one- and multi-element plants was larger for the normalized underwater frontal projected area (15-30% difference in Figure 7 in Publication I) than for the $F_D/A_{tot}$ (10-15%, Publication I).

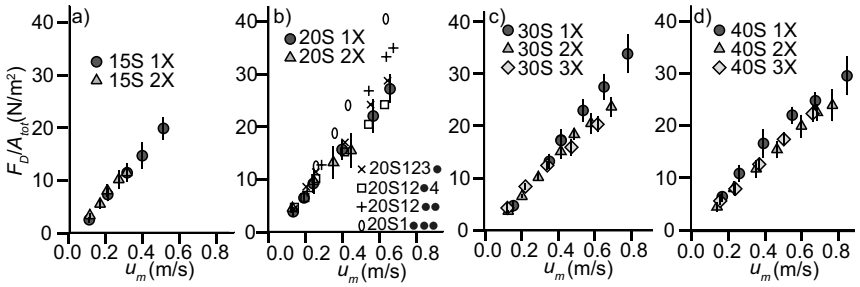


Figure 8. Spatially averaged drag forces $\langle F_D \rangle$ of the vegetation elements normalized with the total one-sided area, $A_{tot}$ for all the investigated setups with the spacing of a) 15 cm, b) 20 cm, c) 30 cm and d) 40 cm. The leaf to stem area ratio $A_L/A_S$ of the 1X, 2X and 3X plants was 18.6. For the plants with varying vertical leaf area distribution $A_L/A_S$ ranged from 3.3 (1●●●) to 13.2 (12●4). The error bars denote the ±1 standard deviation. (Publication I). See Figure 2 for the plant setups.

For the dataset with all the different setups (20S-40S, 1X, 2X, 3X, 123●, 12●4, 12●●, 1●●● in Figure 2) and leaf to stem area ratio ($A_L/A_S$) from 3.3 to 18.6 (Table 1), the Pearson correlation was 0.83 ($p < 0.01$) for $F_D/A_L$ vs. $u$ and 0.90 ($p < 0.01$) for $F_D/A_{tot}$vs. $u$ (Figure 8). The effect of the foliage and stem on the drag is explored in Figure 8b for the plants with varying vertical leaf structure, and thus a varying leaf to stem area ratio (3.3-13.2). For velocities of 0.1-0.3 m/s, the differences between the plants of varying vertical leaf area distribution were small. For the velocities higher than 0.3 m/s, the plants 1●●● with the lowest $A_L/A_S$ of 3.3 deviated the most from the $F_D/A_{tot}$ -$u$ relationship in comparison to the one- and two-element plants ($A_L/A_S =$ 18.6). On the other hand, all the plants with $A_L/A_S$ from 18.6 to 13.2 (1X, 2X, 12●4, 123●) fell close to the same curve. For all 20S setups in Figure 8b, the correlation was 0.89 (p<0.01) for $F_D/A_L$ vs. $u$ and 0.94 (p<0.01) for $F_D/A_{tot}$vs. $u$.

For the experimented natural trees of different sizes (Publication II), the parameterization of the drag forces was further evaluated in terms of the coefficient of variation ($c_v$) by investigating the variation in the drag forces normalized with the different characteristic dimensions (Figure 9). Due to the differences in the size of the trees, the range of measured forces was large (Figure 2 in Publication II), and for instance at a velocity of 1.0 m/s the measured forces in foliated condition ranged between 8 N to 80 N (Figure 10c). Despite the large range of forces, the $F_D$ normalized with total plant area showed small variation in terms of $c_v$, which indicated that the total plant area is a suitable parameter for estimating the drag forces. For all the measured trees in the towing tank ($A_L/A_S$ from 9.6 to 26, Table 2) the normalization of the drag forces with total plant area ($F_D/A_{tot}$) appeared the most accurate (the lowest mean $c_v$), although the difference to $F_F/A_L$ and $F_S/A_S$ was small. The normalization of the drag force with leaf area ($F_D/A_L$) showed similar interspecies variation as $F_D/A_{tot}$, but was characterized by a slightly larger intraspecific (within a single species) variation, which was likely caused by differences in $A_L/A_S$ between the specimens. Overall, in terms of the variation of the normalizations ($c_v$ in Figure 9), the area-based parameterization appeared to be more suitable than the volume- or biomass-based ones. $F_D/A_{tot}$ and $F_S/A_S$

had both the smallest interspecies and intraspecific variation compared to the normalizations with biomass and volume.

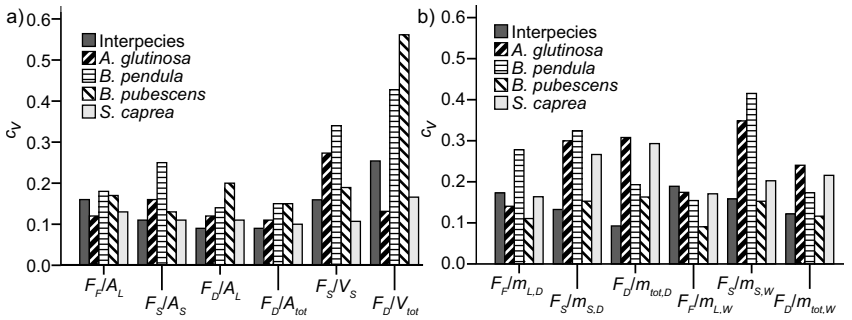


Figure 9. The coefficient of variation for the normalizations with a) the characteristic areas ($A$) and volumes ($V$), and b) the dry ($m_d$) and wet masses ($m_w$). (Publication II).

To further evaluate the difference of $F_D/A_L$ or $F_D/A_{tot}$ for the measured trees (Publication II), linear correlation was tested between $F_D$ and $A_{tot}$ for the lowest measured velocity of 0.1 m/s, for the velocity of 0.5 m/s when most of the reconfiguration had occurred (see Figure 11), and for the velocities of 1.0 m/s and 1.5 m/s. The measured drag forces correlated linearly with $A_{tot}$, and the Pearson correlation was 0.98 ($p < 0.05$) averaged for velocities of 0.1, 0.5, 1.0 m/s (Figure 10) and 1.5 m/s. Similarly, for the defoliated specimens, significant correlation was found between $A_S$ and $F_S$ ($0.97, p < 0.01$). For $F_D$ and $A_L$ the correlation was slightly lower than for $F_D$ and $A_{tot}$ ($0.92, p < 0.01$).

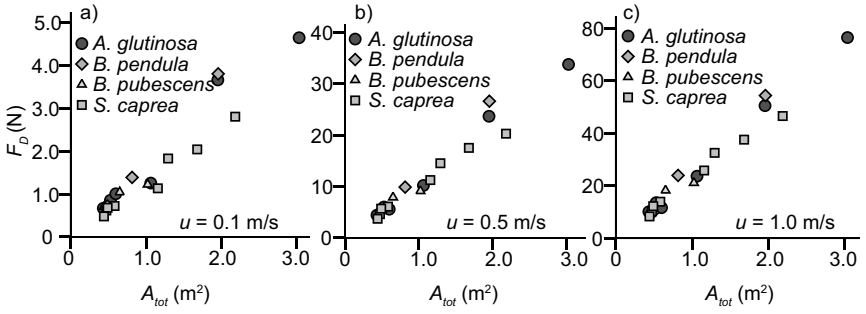


Figure 10. Bulk drag force $F_D$ as a function of total plant area $A_{tot}$ for a) $u$ = 0.1 m/s, b) $u$ = 0.5 m/s and c) $u$ = 1.0 m/s. (data from Publication II).

The reduction of the frontal area and the deflected height of the trees is depicted in Figure 11 with the share of the foliage drag to the total drag ($F_F/F_D$) against velocity (Publication II). At the lowest measured velocity of 0.1 m/s the foliage contributed 70-80% to the total drag (Figure 11a). This share decreased steadily to a velocity of 0.5 m/s and remained approximately 40% for velocities of 0.6 m/s and higher. The frontal projected area in relation to the frontal area at zero velocity ($A_{PW}/A_{PW0}$) was around 70–90% at $u$ = 0.1 m/s and decreased rapidly to circa 35% at 0.6 m/s (Figure 11b). In comparison, for the artificial plant elements (Publication I), the streamlining appeared to reach a maximum at $u$ =

0.6 m/s. The deflected height of the foliated specimens ($H_d$) decreased almost constantly to a velocity of 1.0 m/s (Figure 11d) (Publication II). In contrast to the foliated specimens (Figure 11d), the decrease in $H_{dS}$ of the defoliated specimens was more pronounced at $u = 0.5 - 1.5$ m/s than at the lower velocities (Figure 11c).

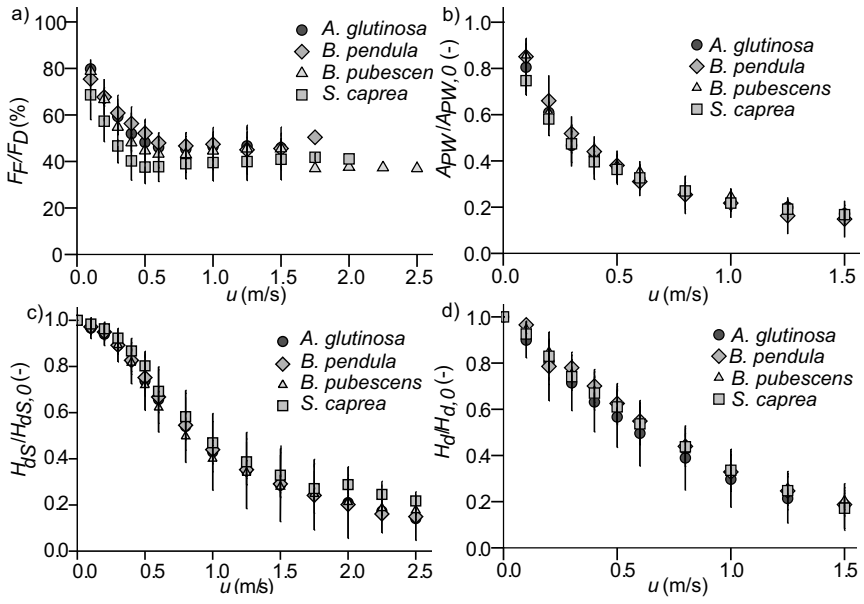


Figure 11. a) The contribution of foliage to the total drag $F_F/F_D$, b) the relative foliated projected area $A_{PW}/A_{PW,0}$, the relative height of the specimen underwater for c) defoliated specimens $H_{d,S}/H_{d,S,0}$ and d) foliated specimens $H_d/H_{d,0}$. (Publication II).

The species-averaged reconfiguration parameters ($\chi$) were derived from the power law regression (Eq. 3, Figure 12) of the drag force and velocity (Publication II). $F_D$ showed less efficient reconfiguration of the foliated tree than the foliage alone with $\chi$ on average $-0.81$ (Figure 8 in Publication II). The foliage drag ($F_F$) showed an almost linear relationship with $u$, as $\chi_F$ was on average $-1.03$ (Figures 3b and 8b in Publication II). By deriving power-type regressions for the defoliated $F_S/A_S$ vs. $u$ (Figure 12b) separately for the velocity ranges of 0.1-0.6 m/s and 0.6-2.5 m/s, it can be observed that $\chi_S$ varies between low ($< 0.6$ m/s) and high ($> 0.6$ m/s) velocities. Figure 11c showed that the stem deflects less at velocities of 0-0.6 m/s than at higher velocities, which may explain the piece-wise behaviour of $F_S/A_S$ vs. $u$ observed from the data in Figure 12b. The $F_S$-$u$ relationship appeared close to a linear for velocities larger than 0.6 m/s ($\chi \approx -1$), whereas for $u < 0.6$ m/s the stem drag vs. $u$ relationship was closer to that for a rigid element ($\chi_S \approx -0.24$) (i.e. less negative $\chi$). The different deflected height ratio of the defoliated and foliated specimens (Figure 11c and d) was attributed to the large impact of foliage on drag at low velocities.

The results showed that other factors in addition to the reduction in frontal projected area contributed to the reconfiguration, as the underwater frontal projected area divided by the frontal projected area in still water ( $A_{PW}/A_{PW0}$ in

Figure 11b) suggested more rigid behaviour (i.e. less negative exponent value) than $\chi$: The exponent of $A_{PW}/A_{PW0}$-$u$ power-type regression was $-0.59$ (from data in Figure 11b) whereas $\chi$ was around $-0.8$ (from data in Figure 12a). This difference of the rate of change in $A_P$ under flow and $F_D$–$u$ power-type regressions may be partially caused by the leaves behind the frontal area impacting the drag (see discussion in Sections 4.1. and 4.3.).

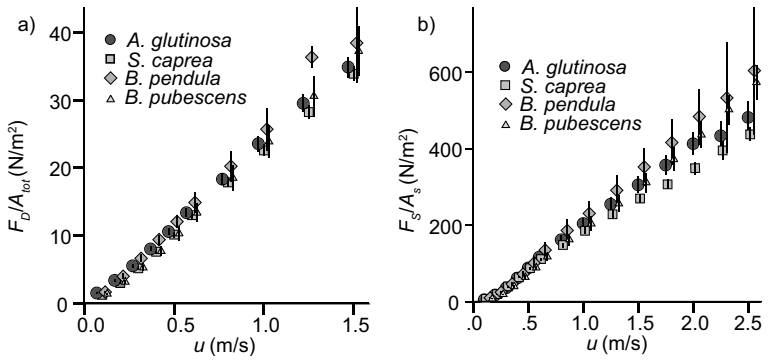


Figure 12. The species-averaged normalized drag forces for a) foliated specimens and b) defoliated specimens. The measured velocities were 0.1-1.5 m/s for foliated and 0.1-2.5 m/s for defoliated specimens. For visual clarity, the data points are slightly shifted horizontally, but equal velocities were measured. Error bars denote ±1 standard deviation. (Publication II).

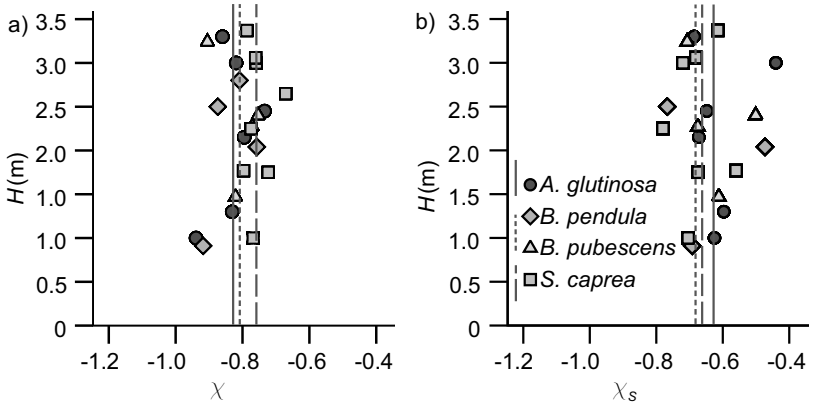


Figure 13. The $\chi$ values for the trees of different heights (and leaf to stem area ratio $A_L/A_S$ between 9.6 and 27), for a) bulk drag and b) stem drag. The lines denote the species-averaged values. (Publication II).

The $\chi$ values for the trees of different sizes (Publication II) were independent on the tree height, as $\chi$ did not deviate notably for specimens of different heights (Figure 13). For the measured tree specimens of heights 0.9–3.4 m, the $A_L/A_S$ varied between 9.6 and 27, and the smaller trees ($< 1.5$ m) were characterized by a larger share of leaves compared to the stem (Figure 7a in Publication II). Thus, the $\chi$ values of the measured trees appeared independent of both $A_L/A_S$ and tree height.

## 3.2 Determination of drag forces

The measurements of different characteristic dimensions enabled the evaluation of the applicability of Eqs. (7), (9) and (10) for the experimented trees of this dissertation (Publication II). The suitability of published parameter values was tested for the measured trees of different sizes (height of 0.9-3.4 m, Publication II). The defoliated specimens were experimented at a velocity range of 0.1-2.5 m/s and the foliated specimens at $u$ = 0.1-1.5 m/s (Publication II), hence the predicted drag is plotted for the corresponding velocity ranges in Figure 14. Figure 14a shows the predicted drag forces with the parameter values derived from the friction factor Eqs. (5) (foliated) and (6) (stem) for 0.23 m tall twigs from a flume study (Västilä and Järvelä 2014). The predicted foliated $F_D$ (Eq. 9) was well in accordance with the measured drag force data (Figure 14), and thus indicated that the twig parameter values by Västilä and Järvelä (2014) could be applied for full scale trees. The averaged error of the predicted foliated bulk $F_D$ vs. measured $F_D$ was 6.4% for *A. glutinosa*, −5.3% for *B. pendula* and 13.4% for *S. caprea* (the parameter values for *S. x rubens* were used for *S. caprea*) (Figure 14a).

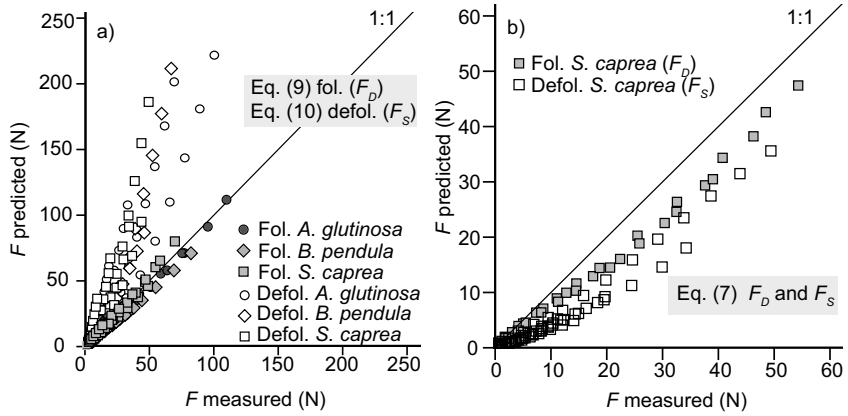


Figure 14. a) The predicted foliated drag $F_D$ and stem drag $F_S$ against the presently measured $F_D$ and $F_S$ using parameter values for circa 23 cm tall twigs of Västilä and Järvelä (2014). The parameter values of $F_D$ were derived using $A_L$ as the characteristic reference area, and hence, the $F_D$ was estimated using $A_L$. b) The predicted $F_D$ and $F_S$ using Eq. (7) with the parameter values of Whittaker et al. (2013). (Publication II).

The predicted stem drag of Eq. (10) for defoliated specimens was over twice the measured one (Figure 14a). This was caused by different velocity ranges used for the parameterization of the literature values than in the present study, and is discussed in more detail in Section 4.3. The reconfiguration parameter $\chi_S$ of the measured full scale trees differed for low velocities ($\chi_{S,low}$, $u$ = 0.1-0.6 m/s, Table 4) and high velocities ($\chi_{S,high}$, $u$ = 0.6-1.5 m/s, Table 4), which was likely caused by the differing reconfiguration for low and high velocities (Figure 11c). The results thus indicated that different $\chi_S$ and $C_{D\chi,S}/u_{\chi,S}^{\chi}$ values are required for low and high flow velocities (Publication II). Such clear velocity dependence of the foliated bulk drag was not found, although $\chi$ slightly changed for higher

values of $u_\chi$ ($\chi \approx -0.95$ for $u$ = 0.6-1.5 m/s and $\chi \approx -1.0$ for $u$ = 1.0-1.5 m/s as an average of all specimens of *S. caprea* and *A. glutinosa*).

The drag forces of foliated specimens predicted with Eq. (7) by applying the parameter values of Whittaker et al. (2013) were 18% lower, and for the defoliated specimens 49% lower than the measured ones (Figure 14b, Publication II).

**Table 4.** The species-averaged parameters for stem drag and bulk drag with $A_S$ and $A_{tot}$, respectively, as the reference area. The $C_D$ corresponds to $C_{D,\chi}/u_\chi^\chi$ and $C_{DS}$ to $C_{D,\chi,S}/u_{\chi,S}^{\chi_S}$. $\chi_{S,low}$ refers to the reconfiguration parameter at low velocities $u$ = 0.1-0.6 m/s and $\chi_{S,high}$ at high velocities $u$ = 0.6-2.5 m/s. (Publication II).

| | Bulk | | Stem | | | | | |
|---|---|---|---|---|---|---|---|---|
| Species | $C_D$ | $\chi$ | $C_{DS}$ | $C_{D,S,high}$ | $C_{D,S,low}$ | $\chi_S$ | $\chi_{S,high}$ | $\chi_{S,low}$ |
| *A. glutinosa* | 0.047 | -0.83 | 0.37 | 0.40 | 0.61 | -0.62 | -1.03 | -0.20 |
| *B. pendula* | 0.052 | -0.84 | 0.43 | 0.42 | 0.62 | -0.66 | -0.96 | -0.36 |
| *B. pubescens* | 0.048 | -0.78 | 0.37 | 0.41 | 0.61 | -0.69 | -0.88 | -0.19 |
| *S. caprea* | 0.045 | -0.76 | 0.34 | 0.36 | 0.59 | -0.66 | -1.05 | -0.22 |

## 3.3 Floodplain topography by means of TLS

Three factors behind the accuracy of TLS derived DTM were explored: vegetation type, its seasonal change, and the point cloud density (Publication III). The test reach averaged mean absolute error, MAE, between the TLS-based DTM for all the window sizes and the reference cross-sections is shown in Figure 15. As the test reach conditions varied strongly depending on the season, the ground-level in most of the cross-sections was generally better detected in May after spring snowmelt than in the autumn, although dense grass debris caused occasional deviations, particularly in Grasses-N. The sparse Bare-M and Willows-M had similar MAE both in May and November. In August, before the grass-cutting with the test reach maintenance, grasses in Bare-M and Willows-M caused larger errors in the ground level than in November after the maintenance (more details in Publication III).

The optimal window size in which laser pulses returned from the ground (Publication III) was investigated for the test reaches with different vegetation cover and in different seasons (Figure 15). The purpose was to analyse the ground point resolution expected in applying TLS for different vegetation conditions. The results of Figure 15 indicated that the ground level can be obtained with MAE = 2-4 cm (30 cm window size) at the beginning of the growing season for floodplain areas with LAI ~3.5 or dry mass per ground area $m_d/A_B$ = 0.4-0.6 (kg/m²) (Grasses-D and Grasses-U). In contrast, for the most densely vegetated sub-reach with Grasses-N (LAI = 9.1), MAE was 7 cm for the largest investigated window size of 100 cm. In November, the TLS scans of the maintained sub-reaches produced reasonable ground level estimates, but for the grassy sub-reaches the MAE was larger than 7 cm. As the lowest reach-averaged MAE was 4 cm for a window size of 50 cm (DTM of May point cloud), the overall accuracy was not sufficient for high-resolution analyses of floodplain topography, e.g. monitoring erosion and deposition processes amidst variable vegetation.

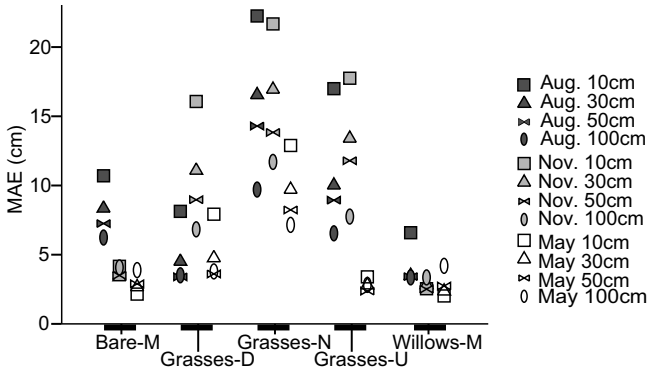


Figure 15. DTM mean absolute error averaged for the sub-reaches in November, August and May (Publication III). The mean absolute error was defined between the TLS based DTM and manually measured points of the cross-section.

The sufficient point cloud density (Publication III) to estimate the ground level of vegetated floodplains is investigated in Figure 16 by reducing the densest point clouds of Grasses-D and Willows-M in to 25, 11 and 6% of the original (100%). Compared to the 25% of the original (50,000 pts/m²), the higher point cloud density improved the DTM accuracy on average 14% and up to 38% (0-2.4 cm). This change in MAE was small particularly for the window size of 30 cm and larger. The reduction of the point cloud in to 6% (1,000 pts/m$^2$) of the original decreased the ground level estimation accuracy by 1-7 cm, on average 50%. The improvement of employing higher scan resolution was the largest for Grasses-D-2 (3-4 cm with the 10 cm window size). Comparing the registered (100%, combined from the scans from both banks) and the individual point clouds (50%, scanned from the left and right banks), showed on average 50% higher MAE for the individual than the registered ones (Figure 16b and Figure 16c).

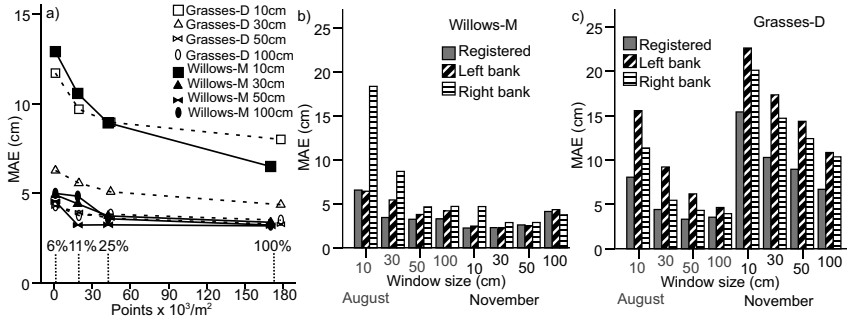


Figure 16. a) The mean absolute errors (MAE) at different point cloud densities (6%, 11%, 25%) of the original (100%) scan for Willows-M and Grasses-D in August, and MAE of the registered (100%) point clouds in comparison to the individual point clouds from the left and right bank scan stations for b) Willows-M and c) Grasses-D (Publication III).

## 3.4 Vegetation properties by means of TLS

This section investigates the application of TLS for obtaining the vegetation properties in the field for both herbaceous vegetation and woody vegetation (Publications III and IV). The TLS-based grass mean height ($H_m$) with 5 cm grid-resolution was 0-100% and on average 38% higher than the $H_m$ estimated from the photographs of the manual reference surveying (Publication III). These differences between TLS and the manual samples were partly attributed to the spatial variability of the vegetation cover, and to the implemented grid resolution. As the horizontal vegetation distribution varied significantly in the sub-reaches (Publication III), the 5 cm grid resolution of DSM overestimated the vegetation heights. Increasing the DSM resolution to 1 cm improved the TLS-based height estimate, as it decreased the TLS-based mean heights 18-36% and on average 25% (Publication III). The resulting difference between TLS-based $H_m$ with 1 cm resolution and manual surveying was on average 8%.

The comparison between the TLS-based fractional vegetation volume ($V_{TLS}$) and fractional grass plant area ($A_{tot}$) is depicted in Figure 17. The results implied that the cumulative vertical vegetation distribution of grasses may be estimated from the TLS-based cumulative volume. The cumulative percentages of the $V_{TLS}$ in comparison to $A_{tot}$ from the manual sampling were similar for Grasses-N and Grasses-U, although for the lowest vertical height sections of Grasses-D there was up to ~50% difference between manual sampling and TLS.

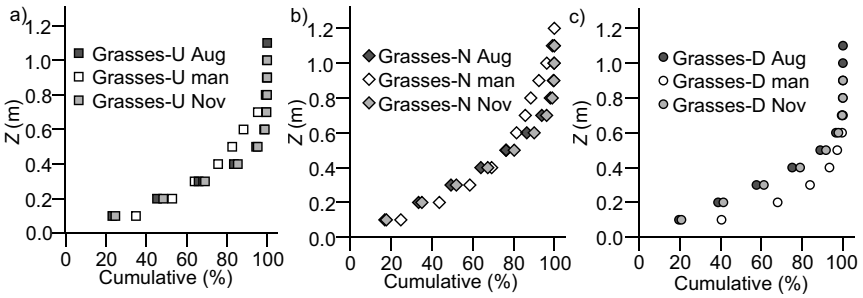


Figure 17. Cumulative percentages of the TLS-based plant volume and the one sided plant area from manual sampling (man.) for 10 cm height increments in: a) Grasses-U, b) Grasses-N, c) Grasses-D. (Publication III).

The relationship between point cloud attributes and manual samples was further evaluated for the quadrates of the 2013 TLS campaign and for the TLS of the trees in laboratory (Figure 18). A linear regression between TLS-based $H_m$ and manually sampled $A_{tot}/A_B$was derived in Figure 18a for the investigated manually sampled 1 m² quadrates consisting of herbaceous vegetation (test reaches 1-3, Figure 6). Similar linear regression existed between the TLS-based herbaceous vegetation volume and $A_{tot}/A_B$. The applied 1 cm grid resolution provided more accurate linear regression ($R^2 = 0.79$) than the 5 cm resolution with $R^2 = 0.64$. The 1 cm grid reflected better the structure of the herbaceous vegetation than the 5 cm grid, which was not able to fully reproduce the variable height distribution and exaggerated the amount of vegetation cover.

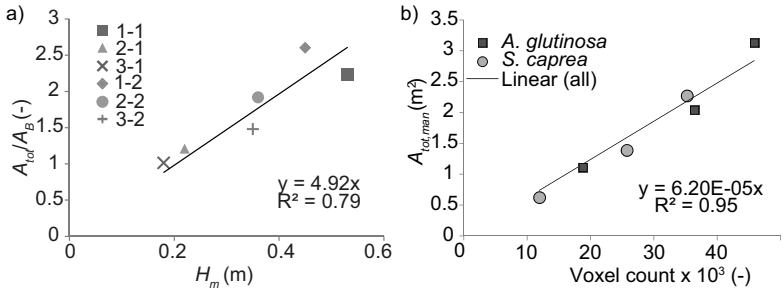


Figure 18. a) Manually determined $A_{tot}/A_B$ as a function of TLS-based mean heights ($H_m$) per ground area for the six field quadrates. b) Manually measured $A_{tot}$ as a function of the count of 1 cm voxels. (Publication IV)

For the investigated specimens of *S. caprea* (SC) and *A. glutinosa* (AG), a linear regression was found for $A_{tot}$ and 1 cm TLS voxel count ($N_{vox}$) (Figure 18b). The linear regression constrained to zero resulted to $A_{tot} = 6.2 \times 10^{-5} N_{vox}$ with $R^2 = 0.95$. Applying 5 cm as well as 10 cm voxels, a similar $R^2$ value was found, but the slope of the linear regression deviated from that of the 1 cm voxels ($A_{tot} = 1.5 \times 10^{-3} N_{vox}$ and $A_{tot} = 5.6 \times 10^{-3} N_{vox}$ for 5 and 10 cm voxels, respectively). The linear regressions of $A_{tot}$ vs. $N_{vox}$ were similar for the investigated *S. caprea* and *A. glutinosa* specimens, although the regressions can be expected to vary for different species due to variability in tree morphology. The goodness of fit was larger for the trees in laboratory than for the herbaceous vegetation in the field site. The Pearson correlation was statistically significant for both but larger for the woody vegetation ($0.98, p < 0.01$) than for the herbaceous vegetation ($0.904, p < 0.05$). This was likely caused by the varying distances of the scanner to the sampling quadrates in the field site (Figure 6).

Figure 19 shows the cumulative vertical distribution of the total plant area from TLS and manual sampling for the six investigated specimens ($A_Z/A_{tot}$). The applicability of the linear regressions was tested for four vertical quartiles ($A_Z$) divided evenly over the specimen height in Figure 19. The TLS-based $A_Z/A_{tot}$ was divided in Figure 19 to eight quartiles to depict the vertical plant distribution over height for the investigated specimens of *S. caprea* (SC) and *A. glutinosa* (AG). The TLS-based cumulative total plant areas ($A_Z/A_{tot}$) estimated for the vertical sections using the linear regression in Figure 18b were 11% larger than the manually measured ones (Figure 19), while the absolute difference was 28%.

The TLS-based height and $A_{tot}/A_B$ surveying based on the linear regressions (Figure 18) allows for determining patches of vegetation as polygonal shapes or gridded values, thus separating individual patches of different heights as well as more homogeneous vegetation cover along the sub-reaches (Figure 12 in Publication III and Figure 8 in Publication IV). The proposed work-flow for the TLS-based estimation of the characteristic vegetation areas is outlined in Figure 20 in Section 4.2.

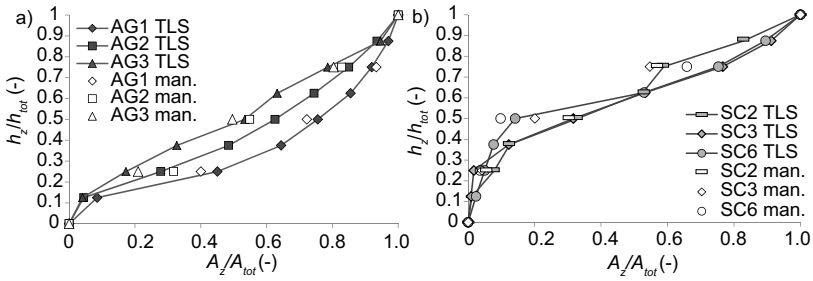


Figure 19. Cumulative vertical distribution of the total plant area from TLS and manual sampling for the three specimens of a) *A. glutinosa* (AG) and b) *S. caprea* (SC). The open symbols denote the manual measurements, and the filled symbols denote the TLS measurements with 1 cm voxels. (Publication IV).

# 4. Discussion

## 4.1 Parameterization of riparian vegetation for hydraulic analyses

The results of Publications I and II indicated that the one-sided total plant area should be used in the hydraulic analyses rather than the frontal projected area ($A_P$). The differences in the drag forces of the plant setups of different densities (10-15%) were smaller than the differences in the projected area (15-30%, Publication I). Thus a straightforward connection between the drag and streamlined frontal projected area assumed in the classical drag force approach was not evident. Most likely, other factors in addition to the streamlined $A_P$, such as the shaded leaves behind it, affect the drag forces (Publication I). These observations with systematically varied vegetation densities confirmed the assumption of Fathi-Moghadam and Kouwen (1997) that the momentum absorbing area is larger than the actual frontal projected area.

In comparison to the one-element plants, a moderate decrease of the drag forces corresponding to an individual plant element was found for the multi-element plants (Publication I). This observed average difference of 10 to 15% suggested that the interactions between the multi-element plants slightly decreased the drag. The difference may be due to the sheltering effects observed to decrease the bulk drag coefficient of cylinders in an array (e.g. Li and Shen 1973; Nepf 1999; Poggi et al. 2004). The upstream plant causes sheltering to the downstream plant for plants adjusted to an array or a group of plants (Li and Shen 1973). This sheltering effect has been observed in a wind tunnel study to be larger for leafy branches than for defoliated ones (Takenake et al. 2010) and can thus cause more drag reduction for the multi-element plants with high leaf area. On the other hand, Dittrich et al. (2012) and Schoneboom et al. (2010) found that the drag forces were 1.25 times larger for plants adjusted to a staggered arrangement than for an isolated single plant. Similarly, the drag forces of the sparsest measured vegetation setup ($A_L/A_B$= 0.23, Table 1) showed lower drag for velocities of 0.65 m/s and 0.85 m/s than the plants in the same spacing with doubled and tripled plant area (two- and three- element plants, Publication I). These contradictory observations of the sheltering may be caused by more efficient reconfiguration of the isolated or sparsely distributed plants, as the 1X setups appeared more rigid by excluding the sparsest one-element plants 40S 1x ($\chi = -0.74$) than all the 1X setups combined (15S-40S 1X) ($\chi = -0.83$).

The parameterization of the drag forces was further analysed for the natural trees by investigating the suitability of the investigated characteristic

dimensions for determining drag forces ($m_d$, $m_W$, $V$, $A_S$, $A_{tot}$, $A_P$, Publication II). Based on the normalization of the drag forces, the total plant area appeared suited for the trees of different sizes with $A_L/A_S$ from 27 to 9.7. $F_S/A_S$ was over tenfold compared to $F_F/A_L$, and thus smaller $A_S$ caused more stem drag than $A_L$ caused foliage drag, which further indicated that the stem drag should be accounted for in the analyses (Publication II). The analyses of the artificial poplars with different vertical leaf area distribution confirmed this assumption (Publication I). However, the difference between $A_L$ and $A_{tot}$ as characteristic reference areas in the drag force equations (Section 2.1.3, Section 4.3) was small for fully foliated specimens, as the leaves constitute a large share of the plants total area (e.g. up to 78% for the willows of Armanini et al. 2005 and 90-96% for the presently measured trees). The foliage drag of the trees showed comparable results with studies for individual leaves in that the leaf shape and surface roughness impact the drag exerted by foliage (Albayrak et al. 2012; Vogel 1989). The leaves of the *S. caprea* were smoother and more elliptic shaped than those of the other investigated species, and the $F_F/A_L$ values were generally 30-50% higher for the other species (Figure 3, Publication II). The $F_S/A_S$ values were on average smaller for *S. caprea* and showed less variation than for the other investigated species, even though differences in the flexural rigidity at mid-stem ($EI_{50}$) between the investigated species were not found (Publication II).

The stem reconfiguration parameter $\chi_S$ appeared to be similar for trees of different sizes, in contrast to the flexural rigidity at mid-stem ($EI_{50}$) (Whittaker et al. 2013 and Zinke 2013, Figure 10b in Publication II). Currently, the drag force formula (Eq. 7 of Whittaker et al (2013) considers foliage through $V$, and stem through $EI$ and $V$, and plant area and drag coefficient as $K_{50}$ parameter which lumps $C_D A_P$ together. $K_{50}$ appeared to correlate with the stem and total area (Figure 12 in Publication II), which implied that $K_{50}$ could be replaced as a product of a constant and characteristic area, e.g. $C_D A_C$. More recently, (Whittaker 2014; Whittaker et al. 2015) modified the drag force formula, and replaced the volume with the frontal projected area. In the present study, the total and stem areas were found to be better resistance predictors than volume or $A_P$. Consequently, it may be viable to modify Eq. (7) to include $A_C H^2$ (Publication II), where $A_C$ is defined as $A_{tot}$ or $A_S$ for foliated and defoliated conditions, respectively. Eq. (7) is based on a modified Cauchy number, which for flexible aquatic vegetation (Luhar and Nepf 2011) include $bl^3$ (where $b$ is blade width and $l$ is blade length). As $EI_{50}$ only considers the bending of the stem, Eq. (7) could be improved by incorporating the flexural rigidity of the leaves in the formulation (Albayrak et al. 2012; Miler et al. 2012).

## 4.2 Vegetation characteristics and floodplain topography from terrestrial laser scanning for hydraulic analyses

The results of Publications I and II indicated that the total plant areas (leaf + stem areas) are feasible characteristic reference areas for foliated woody

vegetation. Subsequently, an approach was proposed (Figure 20) to relate TLS-based point cloud attributes and vegetation characteristics of small sub-areas, and to upscale for larger areas of similar vegetation cover (Publication IV). Obtaining the manually surveyed reference areas in the field is destructive and laborious, particularly for woody vegetation, and hence the reference area was more viable to estimate from high-resolution TLS with 1 mm voxelization rather than manually collecting the samples (Figure 10 in Publication IV). The difference between the 1 mm TLS and manual samples was circa 10% (Figure 10, Publication IV).

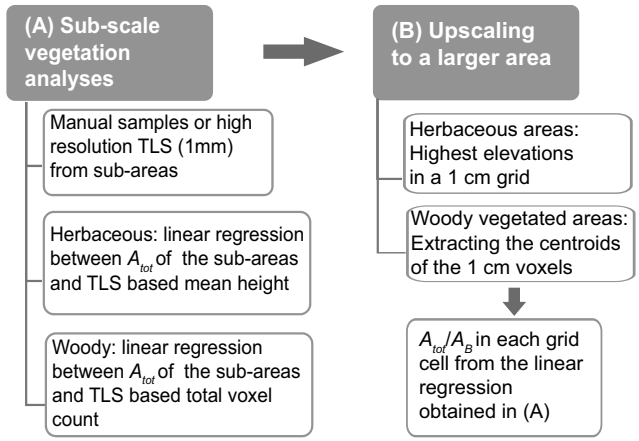


Figure 20. Obtaining vegetation properties: Proposed work-flow of processing multi-station TLS point clouds for hydro-environmental modelling applications. (Publication IV).

For deriving spatial information about physically based vegetation characteristics, TLS proved to be a promising technique in comparison to conventional methods, although different methods are needed to analyse woody and herbaceous type of vegetation (Figure 20). The method based on mean height was adequate for herbaceous vegetation, whereas voxels were applied for woody vegetation (Publications III and IV). The voxels were feasible for the trees, for which the scanning was subject to a small occlusion effect. Dense herbaceous vegetation considerably occludes the laser beam (Publication IV, Guarnieri et al. 2009, Coveney and Fotheringham 2011), which prevented the application of voxels. However, as herbaceous vegetation grows fairly uniformly over height in contrast to woody vegetation, it is adequate to employ the mean height estimated from the highest elevations in a grid cell.

The developed approach (Figure 20, Publication IV) is not limited to TLS, but can be used for point clouds obtained from different LS and surveying methods depending on the data resolution. Structure-from-motion photogrammetry is a low-cost tool advantageous for generating point clouds in remote riverine environments (Westoby et al. 2012). Boat-based mobile laser scanning (BoMMS) provide centimeter resolution point data with a boat speed of 1-2 m/s (Vaaja et al. 2013), and the BoMMS data set can be improved with point clouds from low-altitude unmanned aerial vehicle (UAV) based photogrammetry (Flener et al. 2013). The use of multisource data is superior to sole TLS, though

combining these data requires accurate relative orientation (Rönnholm et al. 2009). For areas of dense vegetation cover, methods that provide point clouds measured from above the vegetation, such as MLS mounted on a backpack or on UAV (Kukko et al. 2012), are able to provide detailed point cloud data of the vegetation and floodplain topography more efficiently than ground-based TLS. To decrease the occlusion in a dense canopy, Hosoi and Omasa (2012) altered the angle of the TLS laser beam by applying mirrors. The developed method (Figure 20, Publication IV) is expected to be useful in the data-analyses of the multisource LS point clouds, as it does not require known scan resolutions or known scan positions (i.e. directions). The determined $A_{tot}/A_B$ in a grid cell (Figure 8 in Publication IV) for different levels of submergence allow for determining the spatially averaged drag forces (Section 4.3). Such vegetation information in vertical and horizontal distributions is useful in 2D and 3D flow and sediment transport models, where the lack of vegetation data is often a limiting factor (e.g. Zinke et al. 2008).

The required point cloud density and the resulting grid resolution depend on the vegetation type and size. For large trees (2-3 m) the voxel sizes of 5 and 10 cm appeared adequate, whereas for the small (~1 m) trees in the field, a 1 cm voxel size was needed (Publication IV). For varying herbaceous vegetation, a 1 cm grid resolution is suitable to estimate vegetation height, but coarser resolution may be adequate for more homogenous vegetation cover (Radtke et al. 2010). For large areas where it is not possible to conduct TLS or MLS for the whole area, it may be feasible to combine the TLS-based total plant areas with ALS data by employing statistical analyses (e.g. Manners et al. 2013).

The TLS-based mean height applied in the present study for estimating $A_{tot}$ (Publications III and IV) pertained to grassy reaches, where individual plants grow fairly uniformly over the height. For herbaceous vegetation and macrophytes, the average vegetation density in terms frontal area per volume is implemented in the drag force equation (Nepf 1999; Huthoff et al. 2007). The results suggested (Publication III) that the fractional TLS-based volume of herbaceous, grassy, vegetation may be used to predict the vertical plant area distribution for different levels of submergence (Figure 17). For grassy vegetation, a model based on the cross-sectional blockage factor successfully predicted the effect of floodplain vegetation on the resistance (Västilä et al. 2015a). This dissertation was among the first investigations to show that the area definitions for estimating vegetative resistance (e.g. Järvelä 2004; Luhar and Nepf 2013; Västilä et al. 2013) are obtainable from the TLS-based point cloud attributes for both herbaceous and woody type of vegetation (Publications III, IV). The linear regressions derived in this study between the $A_{tot}$ and voxel count (Figure 20) provide a starting point for parameterization of trees, as the derived regressions are expected to be applicable in other areas of similar type of woody vegetation.

The estimation of vegetation characteristics requires accurate ground level detection (e.g. from either a validated TLS derived DTM or from other surveying methods), and a classified point cloud with different vegetation types separated to representative classes. The dense vegetation cover caused errors in the

ground detection in the autumn, but the results improved by scanning the area after snowmelt (Publication III). Due to the errors in ground level amidst dense grassy vegetation (Publication III), for high resolution erosion and deposition monitoring in densely vegetated areas TLS needs to be supplemented with other surveying methods. An important factor to be considered in gathering LS data, is the optimal point cloud density (Vaaja et al. 2013), as the large size of the point clouds is challenging for the data-processing. Moreover, the field TLS datasets demonstrated a common characteristic for TLS measurements regarding the high spatial variability of the point cloud density (Publications III and IV). The results revealed that increasing the point cloud density from ~50,000 pts/m$^2$ did not markedly improve the ground level estimate.

The optimal window size for estimating the ground level was further investigated in Publication III. The 30 and 50 cm window sizes appeared the most suitable, whereas the 10 cm window size was too small for dense vegetation areas even with the highest applied scan resolution. In comparison, Guarnieri et al. (2009) defined the optimal filtering window size as 120 cm in a vegetated marsh area. Additional surveying methods of the ground level, such as RTK-GPS, can be incorporated to the point clouds. However, this approach requires a relatively large number of GPS measurements (Coveney and Fotheringham 2011), which are time-consuming to accomplish. Improvements are achieved with novel laser scanning techniques, such as full-waveform laser scanners (e.g. Pirotti et al. 2013), but even these applications do not guarantee ground detection in areas with dense vegetation. For areas with sparse vegetation (Bare-M or Willows-M in the present study, Figure 4), the use of classification methods implemented in TLS software (see e.g. Soininen 2004; Brodu and Lague 2012; Brasington et al. 2012) would improve the DTM accuracy as the ground and vegetation points are clearly distinguishable in these areas. However, for areas of dense vegetation cover minimum TLS elevation methods are feasible (Guarnieri et al. 2009).

The proposed method for deriving the characteristic reference areas (Figure 20) requires that the vegetation points are classified to different vegetation types either by manual or automatic classification. After the vegetation types are distinguished, the mean height or voxel based linear regressions suitable for each vegetation type are applied to derive the plant areas. The geometry-based classification tools designed to distinguish between different types of elements (Brodu and Lague 2012) may be feasible for classifying vegetation types. In a larger scale (e.g. 2×2 m grid) MLS point clouds can be classified as bare, field, shrubs, and canopy layer by exploiting point cloud statistics (mean height, 95th percentile, Saarinen et al. 2013). Laser pulse intensity values are used to classify trees and its species (Holmgren and Persson 2004; Kaasalainen et al. 2007), or the stem (wood material) and foliage of woody vegetation (Béland et al. 2014). Canopy surfaces and tree positions derived from terrestrial and airborne LS as well as the combination of LiDAR, radar and multispectral data provide useful information for defining areas of different vegetation type (Forzieri et al. 2011; Forzieri et al. 2009; Forzieri et al. 2012; Liang and Hyyppä 2013).

## 4.3 Determination of drag forces exerted on woody vegetation

The results of Publication I and II suggested that the vegetative drag force can be estimated with a single drag force formula for different scales of interest (Eq. 12, Figure 21), which is based on the Järvelä (2004) friction factor.

$$F_D = \frac{1}{2}\rho \frac{C_{D\chi}}{u_\chi^\chi} A_C u_C^{2+\chi} \tag{12}$$

In Eq. (12) the effect of reconfiguration is described through the term $C_{D\chi}u_c^\chi/u_\chi^\chi$. The parameter values can be derived for a defoliated or a foliated tree from laboratory investigations, and applied in reach scale. Figure 21 shows the characteristic reference areas ($A_C$) for the different drag force analyses (foliated tree, stem, foliage and individual leaf). For fully foliated specimens for which the leaf area dominates the drag, the results indicated that $A_L + A_S$ should be lumped together to estimate the bulk $F_D$ (Publications I and II). The drag caused by individual leaves was not investigated in this study, but has been evaluated in other studies (Albayrak et al. 2012; Albayrak et al. 2014; Vogel 1989).

The drag force in Eq. (12) can be upscaled to a reach scale by applying the characteristic plant area per unit bed area (Aberle and Järvelä 2015). Consequently, a novel method was developed (Sections 3.4 and 4.2) to estimate the total plant area per ground area. The performance of Eq. (12) and the drag parameterization of trees based on the gathered data and literature is discussed next.

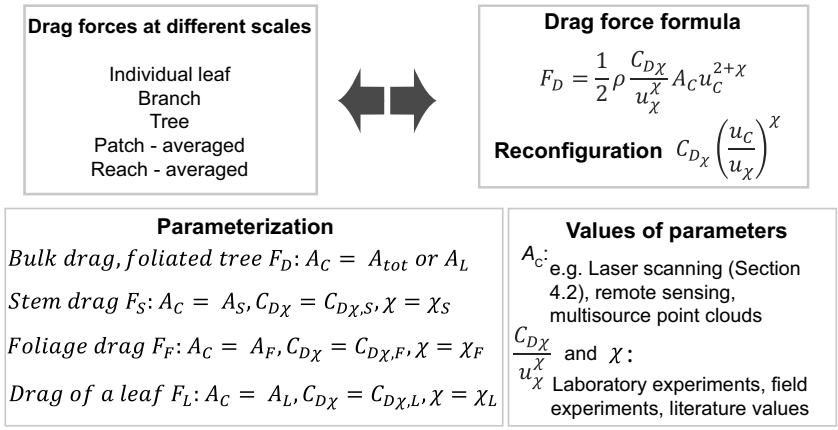


Figure 21. Determination of drag forces in different scales

For fully foliated woody vegetation, the bulk drag force (Eq. 9) could satisfactorily predict the resistance of the artificial poplars with the same parameter values ($\chi, C_{D\chi}/u_\chi^\chi$) for a wide range of vegetation densities (LAI = $A_L/A_B$) (Publication I). For the whole investigated velocity range of 0.1-1.5 m/s in Publication II, the bulk $F_D$ with $A_L$ as reference area produced reasonable results for the trees with parameter values obtained for twigs by Västilä and Järvelä (2014). These observations confirmed the hypotheses behind the towing

tank study (Publication II) that results obtained in flume studies for twigs could be applied for larger trees.

Based on the experimented natural trees, the bulk drag did not depend on the plant scale, as $\chi$ appeared similar for the trees of different sizes (Publication II). In comparison to literature, the reconfiguration was less effective for young ~70 cm *Salix caprea* where $\chi = -0.6$, but more efficient with $\chi$ equal to $-0.9$ for 25 cm high *Salix triandra* × *viminalis* (Järvelä 2006; Järvelä 2004; Järvelä 2002b). In comparison to full-scale trees (Whittaker et al. 2013), $\chi$ was similar to *S. atrocinerea* and *S. alba* of 2-4 m in height, and *A. glutinosa* specimens where $\chi$ was around $-0.82$ and $-0.73$. Although the reconfiguration parameter $\chi$ is implemented in several studies (Järvelä 2004; de Langre 2008; Västilä et al. 2013; Whittaker et al. 2013), this study was the first to show that the same values of bulk $\chi$ and stem $\chi_S$ were applicable for a range of trees of different heights and sizes.

The experiments with the analyses of the streamlined $A_P$ and the deflected tree height revealed the dependence of the $F$ - $u$ relationship on the reconfiguration and bending of the specimens (Publication II). The deflected height ratio of the defoliated specimens changed at around $u = 0.6$ m/s, which did not appear for the foliated specimens. The $F_S$-$u$ relationship was almost linear for velocities higher than 0.5 m/s, but for velocities below 0.6 m/s a closer to squared $F_S$-$u$ relationship existed. The leaves enhanced the reconfiguration at low velocities, indicating that the share of the stem drag in the bulk drag was lower than observed without foliage due to more efficient reconfiguration of foliated trees at low velocities compared to the defoliated specimens. The analyses in Section 3.2 revealed that for fully foliated trees the actual foliage drag at low velocities does not correspond to the $F_F = F_D - F_S$ (as in e.g. Wilson et al. 2010; Dittrich et al. 2012; Whittaker et al. 2013; Västilä and Järvelä 2014), which resulted from the strong effect of foliage on the reconfiguration of the foliated stem (Publication II). Notably, this result does not exclude the use of $F_{tot} = F_F + F_S$, as the combined effect of bulk $F_D$ and $F_S$ is nonetheless accounted for in determining the parameters for $F_F$ ($= F_D - F_S$) from measurements. Early in the spring with the trees having less foliage than later in the growing season, modelling the leaves and stem separately (Västilä and Järvelä 2014) may be particularly useful. The foliage drag differs from the sum of the drag of individual leaves due to streamlining and interactions of leaves attached to a tree (Albayrak et al. 2014; Vogel 1989), and similarly the interaction of the leaves affect the stem drag in foliated conditions.

Aberle and Järvelä (2013) noted that $\chi$ is sensitive to the first measured velocity $u_\chi$. Chapman et al. (2015) obtained similar results for flexible cylindrical elements by estimating $\chi$ for three different velocities 0.1 m/s, 0.216 m/s, and 0.3 m/s. For the foliated trees in this study, $\chi$ was slightly affected by the velocity range and changed from $-0.8$ for $u$ = 0-1.5 m/s to $-1$ for the velocity range of 1-1.5 m/s. Oplatka (1998) observed a close to a linear $F$-$u$ relationship ($\chi = -1$) from experiments conducted with 0.5 m/s increments up to 4 m/s. Wilson et al. (2010) identified a transition zone between low ($u < 0.5$ m/s) and high velocities for both foliated and defoliated specimens (data in Xavier 2009).

This observation of a clear change in $F_D$-$u$ relationship for foliated specimens in addition to the defoliated ones may be attributed to smaller $A_L/A_S$ in Xavier (2009) compared to the present study, but this assumption cannot be verified as $A_L/A_S$ was available for only three specimens of Xavier (2009) (Figure 10 in Publication II). Freeman et al. (2000) observed for broadleaf deciduous shrubs ($H$ = 0.2-1.5 m) that the streamlining started to reach a maximum at a velocity of 1.2 m/s when $F$ began to increase exponentially (squared) with flow velocity, but for 0-1.2 m/s $F$ increased almost linearly. Such a change to exponential increase of $F$ with velocity was not found for the trees in this study. In addition to the moderate changes in the reconfiguration at high velocities, the small quick undulations of the specimens and its leaves may have reduced the drag with increased flow (Albayrak et al. 2012; Nikora 2010).

The effect of tree size on the drag estimation should be further studied for different levels of submergence. The parameter values for foliated $F_D$ are less likely to change than for $F_S$, as the leaves have a significant impact on the reconfiguration (Figure 11). Previous research has shown that the partially submerged stems are likely more rigid compared to fully submerged flow conditions (Armanini et al. 2005). The vertical flow velocity distribution is significantly affected by the vertical leaf area distribution causing the flow velocity to accelerate in the zones of low leaf area (Jalonen et al. 2012). For twigs in a flume, the reconfiguration of the leaves has been observed independent of the level of submergence (Västilä et al. 2013), and thus the same parameter values in Eq. (12) are expected to be applicable for different levels of submergence. To estimate the foliated bulk drag, the vertical distribution of $A_S$ and $A_L$ need to be estimated as a linear profile cannot be assumed (Aberle and Järvelä 2013; Publication IV).

# 5. Conclusions

The dissertation had two main objectives considering the flow resistance of vegetated rivers and floodplains. Firstly, it investigated the parameterization of woody vegetation for determining drag forces and secondly, the applicability of terrestrial laser scanning for obtaining the vegetation parameters of herbaceous and woody vegetation required in the hydro-environmental modelling applications. The conclusions for the specific objectives are highlighted below.

*The effect of plant scale and vegetation density on the estimation of drag forces*

The leaf area ($A_L$) and the total plant areas ($A_{tot}$) were the key parameters for estimating the drag forces of foliated woody vegetation. $A_L$ was feasible independent of the density and distribution of the foliage for specimens with leaf to stem area ratio larger than 13 (Publication I). The frontal projected area was not an adequate parameter, as the leaf area hidden behind the frontal projected area exerted drag and should therefore be taken into account in hydraulic analyses. The distances between the plants did not have a significant impact on the drag of the individual plants at comparable flow velocities, i.e. the interactions between the plants remained approximately constant for the investigated conditions. For vegetation with low leaf to stem area ratio the impact of the stem should not be neglected in estimating the drag (Publications I and II).

A drag force formulation was proposed for woody foliated vegetation with the total plant area and for the stem drag with the stem area as characteristic reference area (Publication II). $A_{tot}$ can be used to estimate the foliated drag for trees of different heights ($H$ = 1-3 m) with $A_L/A_S > 9$ (Publication II). The study was the first to show that the reconfiguration parameter $\chi$ is independent of the tree height ($H$ = 1-3 m), even though the flexural rigidity of the main stem increases with height (Publication II). At low velocities ($u < 0.6$ m/s), the stem drag of foliated trees reduced in comparison to that under the defoliated condition. Hence, the bulk drag approach considering the combined effect of foliage and stem was feasible for fully foliated bushes and trees for which the foliage dominates. For woody vegetation with $A_L/A_S < 6$, the foliage and stem drag should likely be considered separately (Publication I). This may be the case for trees larger than experimented in this study, as variation in the ratio of leaf area to the stem area was found for trees of different sizes, and the share of leaf area appeared to increase for the smallest specimens (Publication II).

For low velocities, the reconfiguration of the stem was less pronounced and $F_S$-$u$ relationship became closer to a squared than at velocities higher than 0.5 m/s. For estimating the stem drag this piece-wise $F_S$-$u$ relationship needs to be taken into account. The foliage drag at low velocities appeared somewhat larger than estimated by $F_F = F_D - F_S$ in contrast to what is assumed in several studies, as the stem drag of foliated trees at low velocities reduces in comparison to the defoliated condition due to more efficient reconfiguration of the stem caused by the foliage.

*TLS-based estimation of floodplain topography: how the type of vegetation including its seasonal change impact the accuracy of the ground level estimate*

The ground level can be estimated for areas with $A_{tot}/A_B$ lower than 3.0 with a mean absolute error of circa 3 cm and an optimal window size of 30 cm (Publication III). The dense vegetation cover causes errors in the ground detection (MAE = 3-12 cm) in the autumn, but the results improve by scanning the area after snowmelt (MAE = 2-4 cm for all the sub-reaches excluding one with $A_{tot}/A_B = 9$). The scanning resolution needs to be assessed according to the study objectives. Increasing the point cloud density to higher than 50,000 pts/m² did not markedly improve the ground level estimate. For the point clouds with higher point cloud density, the DTM accuracy improved from 0% to 38% depending on the window size and the test reach. Due to the errors in ground level amidst dense grassy vegetation, for high resolution erosion and deposition monitoring in densely vegetated areas TLS needs to be supplemented with other surveying methods. Particularly, LS conducted from above the vegetation may improve the DTM considerably, even with lower point cloud densities than utilized in this dissertation.

*TLS-based method to derive the total plant areas of herbaceous and foliated woody vegetation for different levels of submergence*

An approach was developed to relate attributes of the TLS data and the vegetation characteristics of small sub-areas to enable upscaling to larger areas of similar vegetation type (Publication IV). Two alternatives are viable for determining the relationships between the TLS-based attributes and total plant area ($A_{tot}$) of the sub-areas: by millimetre resolution TLS or by collecting manual vegetation samples. In performing the sub-area measurements, the use of TLS is preferable over laborious and destructive manual sampling, in particular for woody vegetation.

Different methods are required for woody and herbaceous type of vegetation. For herbaceous vegetation, the mean heights of the digital surface model were sufficient for determining $A_{tot}$. For woody vegetation, a linear regression based on the voxel count was feasible to estimate both $A_{tot}$ and its vertical distribution. The voxel size of 1 cm is required for describing small thin trees, but for the larger trees 5 and 10 cm voxels are adequate. In estimating the mean heights of the herbaceous vegetation, the 1 cm grid size is required as the 5 cm grid is not

capable of reproducing the varying height distributions. Due to the variability in the herbaceous vegetation cover, the linear regression derived between $A_{tot}$ and TLS-based mean heights is considered as site specific.

Overall, the results of the LS-based monitoring of vegetation properties combined with physically-based characterization of drag forces are useful in various hydro-environmental modelling applications, such as predicting water levels, determining flow velocities for the investigation of sediment and nutrient processes or investigating environmental flows in vegetated rivers.

The comprehensive tree property and force data comprised a novel data set more extensive than those in the existing literature, and thus allowed evaluation of different plant parameterizations for physically-based modelling. Comparing TLS to manual surveying provided new knowledge of the TLS for determining floodplain topography in areas of varying vegetation cover, and for different seasons. The new approach to estimate the total plant areas from TLS provided a solution for obtaining high-resolution data of the horizontal and vertical distribution of both woody and herbaceous type of vegetation.

It remains to be investigated to what extent the parameter values of $\chi$ and $C_{D\chi}$ are species-specific and how they depend on growing conditions. For the estimation of TLS-based total plant areas, it is expected that the regressions acquired for woody vegetation can be extended to other sites with similar vegetation type, though it should be investigated how these relationships vary for trees of different sizes and ages.

# References


Aberle, J., and Järvelä, J. (2013). "Flow Resistance of Emergent Rigid and Flexible Floodplain Vegetation." J. Hydraul. Res., 51(1), 33-45.

Aberle, J., and Järvelä, J. (2015). "Hydrodynamics of Vegetated Channels." Rivers – Physical, Fluvial and Environmental Processes, GeoPlanet: Earth and Planetary Sciences, Springer, Switzerland, 519-541.

Albayrak, I., Nikora, V., Miler, O., O'Hare, M. (2012). "Flow-Plant Interactions at a Leaf Scale: Effects of Leaf Shape, Serration, Roughness and Flexural Rigidity." Aquat. Sci., 74(2), 267-286.

Albayrak, I., Nikora, V., Miler, O., O'Hare, M. (2014). "Flow–plant Interactions at Leaf, Stem and Shoot Scales: Drag, Turbulence, and Biomechanics." Aquat. Sci., 76(2), 1-26.

Antonarakis, A. S., Richards, K. S., Brasington, J., Muller, E. (2010). "Determining Leaf Area Index and Leafy Tree Roughness using Terrestrial Laser Scanning." Water Resour. Res., 46(6), W06510.

Armanini, A., Righetti, M., Grisenti, P. (2005). "Direct Measurement of Vegetation Resistance in Prototype Scale." J. Hydraul. Res., 43(5), 481-487.

Béland, M., Widlowski, J., Fournier, R. A. (2014). "A Model for Deriving Voxel-Level Tree Leaf Area Density Estimates from Ground-Based LiDAR." Environ. Modell. Softw., 51(0), 184-189.

Brasington, J., Vericat, D., Rychkov, I. (2012). "Modeling River Bed Morphology, Roughness, and Surface Sedimentology using High Resolution Terrestrial Laser Scanning." Water Resour. Res., 48(11), W11519.

Bréda, N. J. J. (2003). "Ground-Based Measurements of Leaf Area Index: A Review of Methods, Instruments and Current Controversies." Journal of Experimental Botany, 54(392), 2403-2417.

Brodu, N., and Lague, D. (2012). "3D Terrestrial Lidar Data Classification of Complex Natural Scenes using a Multi-Scale Dimensionality Criterion: Applications in Geomorphology." ISPRS J Photogramm Remote Sens., 68, 121-134.

Chapman, J. A., Wilson, B. N., Gulliver, J. S. (2015). "Drag Force Parameters of Rigid and Flexible Vegetal Elements." Water Resour. Res.,51 (5), 3292–3302.

Chow, V. T. (1959). Open-Channel Hydraulics, McGraw-Hill, NewYork, NY.

Coveney, S., and Fotheringham, A. S. (2011). "Terrestrial laser scan error in the presence of dense ground vegetation." Photogramm. Rec., 26 (135), 307–324.

Cowan, W. L. (1956). "Estimating Hydraulic Roughness Coefficients." Agr. Eng., 37(7), 473-475.

Curran, J. C., Hession, W. C. (2013). "Vegetative Impacts on Hydraulics and Sediment Processes Across the Fluvial System." J. Hydrol., 505, 364-376.

Dittrich, A., Aberle, J., Schoneboom, T. (2012). "Drag Forces and Flow Resistance of Flexible Riparian Vegetation." Environmental Fluid Mechanics: Memorial Colloquim on Environmental Fluid Mechanics in Honour of Proferssor Gerhard H. Jirka. CRC Press, London, 195-215.

Eaton, B. C., and Giles, T. R. (2009). "Assessing the Effect of Vegetation-Related Bank Strength on Channel Morphology and Stability in Gravel-Bed Streams using Numerical Models." Earth Surf. Process. Landforms, 34(5), 712-724.

Fathi-Maghadam, M., Kouwen, N. (1997). "Nonrigid, Nonsubmerged, Vegetative Roughness on Floodplains." J. Hydraul. Eng., 123(1), 51-57.
Fischer-Antze, T., Stoesser, T., Bates, P., Olsen, N. R. B. (2001). "3D Numerical Modelling of Open-Channel Flow with Submerged Vegetation." J. Hydraul. Res., 39(3), 303-310.
Flener, C.; Vaaja, M.; Jaakkola, A.; Krooks, A.; Kaartinen, H.; Kukko, A.; Kasvi, E.; Hyyppä, H.; Hyyppä, J.; Alho, P. (2013) "Seamless Mapping of River Channels at High Resolution Using Mobile LiDAR and UAV-Photography." Remote Sens. 5(12), 6382-6407.
Folkard, A. M. (2011). "Vegetated flows in their environmental context: A review." Proc. ICE - Engineering and Computational Mechanics. 164(1), 3-24.
Forzieri, G., Guarnieri, L., Vivoni, E. R., Castelli, F., Preti, F. (2009). "Multiple Attribute Decision Making for Individual Tree Detection using High-Resolution Laser Scanning." For. Ecol. Manage., 258(11), 2501-2510.
Forzieri, G., Moser, G., Vivoni, E., Castelli, F., Canovaro, F. (2010). "Riparian Vegetation Mapping for Hydraulic Roughness Estimation using very High Resolution Remote Sensing Data Fusion." 136(11), 855-867.
Forzieri, G., Guarnieri, L., Vivoni, E. R., Castelli, F., Preti, F. (2011). "Spectral-ALS Data Fusion for Different Roughness Parameterizations of Forested Floodplains." River Res. Appl., 27(7), 826-840.
Forzieri, G., Castelli, F., Preti, F. (2012). "Advances in Remote Sensing of Hydraulic Roughness." Int. J. Remote Sens., 33(2), 630-654.
Freeman, G. E., Rahmeyer, W. H., Copeland, R. R. (2000). "Determination of Resistance due to Shrubs and Woody Vegetation", ERDC/CHL TR-00-25, US Army Corps of Engineers, Engineer Research and Development Center., 64.
Frostick, L. E., McLelland, S., Mercer, T. (2011). "Ecological Experiments." Users Guide to Physical Modelling and Experimentation: Experience of the HYDRALAB Network, CRC Press, Balkema, Leiden, The Netherlands, 128-170.
Green, J. C. (2005)."Comparison of blockage factors in modelling the resistance of channels containing submerged macrophytes." River Res. Applic., 21(6), 671–686.
Green, J.C. (2006). "Effect of macrophyte spatial variability on channel resistance", Adv. Water Resour., 29(3) 426-438.
Guarnieri, A., Vettore, A., Pirotti, F., Menenti, M., Marani, M. (2009). "Retrieval of Small-Relief Marsh Morphology from Terrestrial Laser Scanner, Optimal Spatial Filtering, and Laser Return Intensity." Geomorphology, 113(1–2), 12-20.
Gurnell, A. M., van Oosterhout, M. P., de Vlieger, B., Goodson, J. M. (2006). "Reach-Scale Interactions between Aquatic Plants and Physical Habitat: River Frome, Dorset." River Res. Appl., 22(6), 667-680.
Helmiö, T. (2002). "Unsteady 1D Flow Model of Compound Channel with Vegetated Floodplains." J. Hydrol., 269(1–2), 89-99.
Helmiö, T. (2004). Effects of Cross-Sectional Geometry, Vegetation and Ice on Flow Resistance and Conveyance of Natural Rivers, Doctoral dissertation Ed., Department of Civil and Environmental Engineering, Espoo, Finland.
Heritage, G. L., and Large, A. R. G. (2009). Laser Scanning for the Environmental Sciences, Blackwell Publishing Ltd., UK.
Hodge, R., Brasington, J., Richards, K. (2009). "In Situ Characterization of Grain-Scale Fluvial Morphology using Terrestrial Laser Scanning." Earth Surf. Process. Landforms, 34(7), 954-968.
Hoerner, S. (1965). Fluid-Dynamic Drag, Brick Town, NJ, USA.

Hohenthal, J., Alho, P., Hyyppä, J., Hyyppä, H. (2011). "Laser Scanning Applications in Fluvial Studies." Progress in Physical Geography, 35(6), 782-809.
Holmgren, J., and Persson, Å. (2004). "Identifying Species of Individual Trees using Airborne Laser Scanner." Remote Sens. Environ., 90(4), 415-423.
Horritt, M. S., and Bates, P. D. (2002). "Evaluation of 1D and 2D Numerical Models for Predicting River Flood Inundation." J. Hydrol., 268(1–4), 87-99.
Hosoi, F., and Omasa, K. (2006). "Voxel-Based 3-D Modeling of Individual Trees for Estimating Leaf Area Density using High-Resolution Portable Scanning Lidar", IEEE Transactions on Geoscience and Remote Sensing, 44, 3610-3618.
Hosoi, F., and Omasa, K. (2012). "Estimation of Vertical Plant Area Density Profiles in a Rice Canopy at Different Growth Stages by High-Resolution Portable Scanning Lidar with a Lightweight Mirror." ISPRS J. Photogramm. Remote Sens., 74(0), 11-19.
Huthoff, F. (2007). Modeling Hydraulic Resistance of Floodplain Vegetation, PhD thesis, University of Twente, Enschede, the Netherlands.
Huthoff, F., Augustijn, D. C. M., Hulscher, S. J. M. H. (2007). "Analytical Solution of the Depth-Averaged Flow Velocity in Case of Submerged Rigid Cylindrical Vegetation." Water Resour. Res., 43(6), W06413.
Hyyppä, J. (2011). "State of the art in laser scanning." Proc., Photogrammetric Week'11, Wichmann, VDE, 203-216.
Jalonen, J., Järvelä, J., Aberle, J. (2012). "Vegetated flows: Drag force and velocity profiles for foliated plant stands." Proc., River Flow 2012, International Conference on Fluvial Hydraulics, Taylor & Francis, San José, Costa Rica, 233-239.
James, C. S., Goldbeck, U. K., Patini, A., Jordanova, A. A. (2008). "Influence of Foliage on Flow Resistance of Emergent Vegetation." J. Hydraul. Res., 46(4), 536-542.
Järvelä, J. (2002a). "Determination of flow resistance of vegetated channel banks and floodplains." Proc., Int. Conf. River Flow 2002, Swets & Zeitlinger, Louvain-La-Neuve, Belgium, 311-318.
Järvelä, J. (2002b). "Flow Resistance of Flexible and Stiff Vegetation: A Flume Study with Natural Plants." J. Hydrol., 269(1–2), 44-54.
Järvelä, J. (2004). "Determination of Flow Resistance Caused by Non-submerged Woody Vegetation." Intl. J. River Basin Manag., 2(1), 61-70.
Järvelä, J. (2006). "Vegetative flow resistance: Characterization of woody plants for modelling applications." Proc., World Water and Environmental Resources Congress, ASCE, Omaha, 1-10.
Johnson, M. F., Thomas, R. E., Dijkstra, J. T., Paul, M., Penning, W. E., Rice, S. P. (2014). "Using Surrogates, Including Scaling Issues, in Laboratory Flumes and Basins." Users Guide to Ecohydraulic Modelling and Experimentation: Experience of the Ecohydraulic Researech Team (PISCES) of the HYDRALAB Network. CRC Press, Balkema, Leiden, The Netherlands, 23-41.
Kaasalainen, S., Lindroos, T., Hyyppä, J. (2007). "Toward Hyperspectral Lidar: Measurement of Spectral Backscatter Intensity with a Supercontinuum Laser Source." Geoscience and Remote Sensing Letters, IEEE, 4(2), 211-215.
Katul, G. G., Poggi, D., Ridolfi, L. (2011). "A Flow Resistance Model for Assessing the Impact of Vegetation on Flood Routing Mechanics." Water Resour. Res., 47(8), W08533.
Kouwen, N., Unny, T. E., Hill, H. M. (1969). "Flow Retardance in Vegetated Channels." Journal of the Irrigation and Drainage Division, 95(2), 329-344.
Kouwen, N., and Unny, T. E. (1973). "Flexible Roughness in Open Channels." J. Hydraulic. Div., 99(5), 713-728.

Kouwen, N., and Fathi-Moghadam, M. (2000). "Friction Factors for Coniferous Trees Along Rivers." J. Hydraul. Eng., 126(10), 732-740.
Kukko, A., Kaartinen, H., Hyyppä, J., Chen, Y. (2012). "Multiplatform Mobile Laser Scanning: Usability and Performance." Sensors, 12(9), 11712-11733.
de Langre, E. (2008). "Effects of Wind on Plants." Annu. Rev. Fluid Mech., 40(1), 141-168.
Li, R., and Shen, H. W. (1973). "Effect of Tall Vegetations on Flow and Sediment." J. Hydraulic. Div. , ASCE, 99(5), 793-814.
Liang, X., and Hyyppä, J. (2013). "Automatic Stem Mapping by Merging several Terrestrial Laser Scans at the Feature and Decision Levels." Sensors, 13(2), 1614-1634.
Lichti, D. D., Gordon, S. J., Stewart, M. P. (2002). "Ground-Based Laser Scanners: Operation, Systems and Applications." Geomatica, 56(1), 21-33.
Luhar, M., and Nepf, H.M. (2011). "Flow-Induced Reconfiguration of Buoyant and Flexible Aquatic Vegetation." Limnol. Oceanogr., 56(6), 2003-2017.
Luhar, M., and Nepf, H. M. (2013). "From the Blade Scale to the Reach Scale: A Characterization of Aquatic Vegetative Drag." Adv. Water Resour., 51, 305-316.
Manners, R., Schmidt, J., Wheaton, J. M. (2013). "Multiscalar Model for the Determination of Spatially Explicit Riparian Vegetation Roughness." Earth Surf. Process. Landforms, 118, 65-83.
Marjoribanks, T. I., Hardy, R. J., Lane, S. N., Parsons, D. R. (2014). "High-Resolution Numerical Modelling of Flow—vegetation Interactions." J. Hydraul. Res., 52(6), 775-793.
Merritt, D. M., Scott, M. L., Leroy Poff, N., Auble, G. T., Lytle, D. A. (2010). "Theory, Methods and Tools for Determining Environmental Flows for Riparian Vegetation: Riparian Vegetation-Flow Response Guilds." Freshwat. Biol., 55(1), 206-225.
Miler, O., Albayrak, I., Nikora, V., O'Hare, M. (2012). "Biomechanical Properties of Aquatic Plants and their Effects on Plant–flow Interactions in Streams and Rivers." Aquat. Sci., 74(1), 31-44.
Morsdorf, F., Kötz, B., Meier, E., Itten, K. I., Allgöwer, B. (2006). "Estimation of LAI and Fractional Cover from Small Footprint Airborne Laser Scanning Data Based on Gap Fraction." 104(1), 50-61.
Morvan, H., Knight, D., Wright, N., Tang, X., Crossley, A. (2008). "The Concept of Roughness in Fluvial Hydraulics and its Formulation in 1D, 2D and 3D Numerical Simulation Models." Journal of Hydraulic Research, 46(2), 191-208.
Nepf, H. M. (1999). "Drag, Turbulence, and Diffusion in Flow through Emergent Vegetation." Water Resour. Res., 35(2), 479-489.
Nepf, H.M., and Ghisalberti, M. (2008). "Flow and Transport in Channels with Submerged Vegetation." Acta Geophysica, 56(3), 753-777.
Nikora, V. (2010). "Hydrodynamics of Aquatic Ecosystems : An Interface between Ecology, Biomechanics and Environmental Fluid Mechanics." River Res. Appl., 26(4), 367-384.
Oplatka, M. (1998). "Stabilität Von Weidenverbauungen an Flussufern." Doctoral thesis, Mitt. Versuchsanstalt für Wasserbau, Hydrologie und Glaziologie, No. 156, ETH Zürich, Switzerland, p. 217.
Palmer, V. J. (1945). "A Method for Designing Vegetated Waterways." Agric. Eng., 26(12), 516-520.
Palmer, M., Allan, J. D., Meyer, J., Bernhardt, E. S. (2007). "River Restoration in the Twenty-First Century: Data and Experimental Knowledge to Inform Future Efforts." Restor. Ecol., 15(3), 472-481.

Pasche, E., and Rouvé, G. (1985). "Overbank Flow with Vegetatively Roughned Floodplains." J. Hydraul. Eng., 111(9), 1262-1278.
Petryk, S., and Bosmajian, G. B. (1975). "Analysis of Flow through Vegetation." J. Hydraul. Div., 101, 871-884.
Pirotti, F., Guarnieri, A., and Vettore, A. (2013). "Ground filtering and vegetation mapping using multi-return terrestrial laser scanning." ISPRS J. Photogramm. Remote Sens., 76, 56–63.
Poggi, D., Porporato, A., Ridolfi, L., Albertson, J. D., Katul, G. G. (2004). "The Effect of Vegetation Density on Canopy Sub-Layer Turbulence." Bound. -Layer Meteorol., 111(3), 565-587.
Radtke, P. J., and Bolstad, P. V. (2001). "Laser Point-Quadrat Sampling for Estimating Foliage-Height Profiles in Broad-Leaved Forests." Can. J. Forest Res., 31(3), 410-418.
Radtke, P. J., Boland, H. T., Scaglia, G. (2010). "An Evaluation of Overhead Laser Scanning to Estimate Herbage Removals in Pasture Quadrats." Agric. for. Meteorol., 150(12), 1523-1528.
Resop, J., and Hession, W. (2010). "Terrestrial Laser Scanning for Monitoring Streambank Retreat: Comparison with Traditional Surveying Techniques." J. Hydraul. Eng., 136(10), 794-798.
Resop, J. P., Kozarek, J. L., Hession, W. C. (2012). "Terrestrial Laser Scanning for Delineating in-Stream Boulders and Quantifying Habitat Complexity Measures." Photogramm. Eng. Remote Sensing, 78(4), 363-371.
Richardson, D. M., Holmes, P. M., Esler, K. J., Galatowitsch, S. M., Stromberg, J. C., Kirkman, S. P., Pyšek, P. and Hobbs, R. J. (2007), "Riparian vegetation: degradation, alien plant invasions, and restoration prospects." Divers. Distrib., 13(1), 126–139.
Righetti, M., and Armanini, A. (2002). "Flow Resistance in Open Channel Flows with Sparsely Distributed Bushes." J. Hydrol., 269(1–2), 55-64.
Ritchie, J. C. (1996). "Remote Sensing Applications to Hydrology: Airborne Laser Altimeters." Hydrolog. Sci. J., 41(4), 625-636.
Rönnholm, P., Hyyppä, H., Hyyppä, J., Haggrén, H. (2009). "Orientation of Airborne Laser Scanning Point Clouds with Multi-View, Multi-Scale Image Blocks." Sensors, 9(8), 6008-6027.
Rouse, H., and Ince, S. (1957). History of Hydraulics, Dover Publications Inc., New York.
Rouse, H., (1965). "Critical analyses of open channel resistance." J. Hydr. Eng. Div. ASCE, 91(4), 1-23.
Rouse, H., and Hon, M. (1980). "Some Paradoxes in the History of Hydraulics." J. Hydr. Eng. Div. ASCE, 106(6), 1077-1084.
Rusu, R. B., Marton, Z. C., Blodow, N., Dolha, M., Beetz, M. (2008). "Towards 3D Point Cloud Based Object Maps for Household Environments." Semantic Knowledge in Robotics, 56(11), 927-941.
Rychkov, I., Brasington, J., Vericat, D. (2012). "Computational and Methodological Aspects of Terrestrial Surface Analysis Based on Point Clouds." Comput. Geosci., 42, 64-70.
Saarinen, N., et al. (2013). "Area-based approach for mapping and monitoring riverine vegetation using mobile laser scanning." Remote Sens., 5 (10), 5285–5303.
Sagnes, P. (2010). "Using Multiple Scales to Estimate the Projected Frontal Surface Area of Complex Three-Dimensional Shapes such as Flexible Freshwater Macrophytes at Different Flow Conditions." Limnol. Oceanogr. Methods, 8, 474-483.

Saldi-Caromile, K., Bates, K. K., Skidmore, P., Barenti, J., Pineo, D. (2004). Stream Habitat Restoration Guidelines: Final Draft. Co-published by the Washington Departments of Fish and Wildlife and Ecology and the U.S. Fish and Wildlife Service., Olympia, Washington.

Schoneboom, T., Aberle, J. and Dittrich, A. (2010). “Hydraulic resistance of vegetated flows: Contribution of bed shear stress and vegetative drag to total hydraulic resistance”, Proc. River Flow 2010, Braunschweig, Germany, 269-276.

Schoneboom, T. (2011). "Widerstand Flexibler Vegetation Und Sohlenwiderstand in Durchströmten Bewuchsfeldern." Doctoral thesis, Mitt. Leichtweiß-Institut für Wasserbau No. 157, Braunschweig, Technische Universität Braunschweig, Germany.

Schnauder, I. Wilson, C.A.M.E. (2009). “Discussions”, J. Hydr. Res., 47(3), 384-386.

Shucksmith, J. D., Boxall, J. B., Guymer, I. (2010). "Effects of Emergent and Submerged Natural Vegetation on Longitudinal Mixing in Open Channel Flow." Water Resour. Res., 46(4), W04504.

Simon, A., and Collison, A. J. C. (2002). "Quantifying the Mechanical and Hydrologic Effects of Riparian Vegetation on Streambank Stability." Earth Surf. Process. Landforms, 27(5), 527-546.

Smith, M. W., and Vericat, D. (2013). "Evaluating Shallow-Water Bathymetry from through-Water Terrestrial Laser Scanning Under a Range of Hydraulic and Physical Water Quality Conditions." River Res. Appl., 30(7), 905-924.

Soininen, A. (2004). "Terrascan user’s guide", Terrasolid, Helsinki, 158.

Statzner, B., Lamouroux, N., Nikora, V., Sagnes, P. (2006). "The Debate about Drag and Reconfiguration of Freshwater Macrophytes: Comparing Results obtained by Three Recently Discussed Approaches." Freshwater Biol., 51(11), 2173-2183.

Stoesser, T., Wilson, C. A. M. E., Bates, P. D., Dittrich, A. (2003). "Application of a 3D Numerical Model to a River with Vegetated Floodplains ." J. Hydroinformatics, 5, 99-112.

Stone, M. C., Chen, L., Kyle McKay, S., Goreham, J., Acharya, K., Fischenich, C., Stone, A. B. (2013). "Bending of Submerged Woody Riparian Vegetation as a Function of Hydraulic Flow Conditions." River Res. Appl., 29(2), 195-205.

Straatsma, M. W., and Baptist, M. J. (2008). "Floodplain Roughness Parameterization using Airborne Laser Scanning and Spectral Remote Sensing." Remote Sens. Environ., 112(3), 1062-1080.

Straatsma, M. W., Warmink, J. J., Middelkoop, H. (2008). "Two Novel Methods for Field Measurements of Hydrodynamic Density of Floodplain Vegetation using Terrestrial Laser Scanning and Digital Parallel Photography." Int. J. Remote Sens., 29(5), 1595-1617.

Takenake, H. , Tanaka, N. , Htet, P. M. , Yagisawa, J. (2010). “Wind tunnel experiments on direct measurement of drag force of real tree trunks and branches and their sheltering effects at high Reynolds numbers.” Proc., 8th Int. Symposium on Ecohydraulics 2010, Korea Water Resources Association, Seoul, 1520–1525.

Vaaja, M., Kukko, A., Kaartinen, H., Kurkela, M., Kasvi, E., Flener, C., Hyyppä, H., Hyyppä, J., Järvelä, J., Alho, P. (2013). "Data Processing and Quality Evaluation of a Boat-Based Mobile Laser Scanning System." Sensors, 13(9), 12497-12515.

Vargas-Luna, A., Crosato, A., Uijttewaal, W. S. J. (2015). "Effects of Vegetation on Flow and Sediment Transport: Comparative Analyses and Validation of Predicting Models." Earth Surf. Process. Landforms, 40(2), 157–176.

Vogel, S. (1984). "Drag and Flexibility in Sessile Organisms." Am. Zool., 24(1), 37-44.

Vogel, S. (1989). "Drag and Reconfiguration of Broad Leaves in High Winds." J. Exp. Bot., 40(8), 941-948.
Vollsinger, S., Mitchell, S.J., Byrne, K.E., Novak, M.D., Rudnicki, M. (2005). "Wind tunnel measurements of crown streamlining and drag relationships for several hardwood species." Can. J. Forest Res., 35(5), 1238-1249
Västilä, K., Järvelä, J., Aberle, J., Schoneboom, T. (2011). “Vegetative drag in natural, foliated plant stands.” Proc., 34th IAHR World Congress, Engineers Australia, Canberra, 2978–2985.
Västilä, K., Järvelä, J., Aberle, J. (2013). "Characteristic Reference Areas for Estimating Flow Resistance of Natural Foliated Vegetation." J. Hydrol., 492, 49-60.
Västilä, K., and Järvelä, J. (2014). "Modeling the Flow Resistance of Woody Vegetation using Physically Based Properties of the Foliage and Stem." Water Resour. Res., 50(1), 229-245.
Västilä, K., Järvelä, J., Jalonen, J. (2015a). "Effect of Floodplain Vegetation on Flow and Transport of Cohesive Particles in an Environmental Two-Stage Channel." 36th IAHR World Congress, 28 June – 3 July, 2015, the Hague, the Netherlands.
Västilä, K., Järvelä, J., Koivusalo, H. (2015b). "Flow-Vegetation-Sediment Interaction in a Cohesive Compound Channel." J. Hydraul. Eng., 04015034.
Wehr, A., and Lohr, U. (1999). "Airborne Laser Scanning—an Introduction and Overview." ISPRS J. Photogramm. Remote Sens., 54(2–3), 68-82.
Weissteiner, C., Rauch, H. P., Jalonen, J., Järvelä, J. (2013). "Spatial-structural analysis of woody riparian vegetation for hydraulic considerations." Proc., 35th IAHR World Congress, Tsinghua University Press., Chengdu, China, 11.
Weissteiner, C., Jalonen, J., Järvelä, J., Rauch, H. P. (2015). "Spatial-structural properties of woody riparian vegetation with a view to reconfiguration under hydrodynamic loading." Ecol. Eng., accepted.
Westoby, M. J., Brasington, J., Glasser, N. F., Hambrey, M. J., Reynolds, J. M. (2012). "'Structure-from-Motion' Photogrammetry: A Low-Cost, Effective Tool for Geoscience Applications." Geomorphology, 179, 300-314.
Whittaker, P., Wilson, C., Aberle, J., Rauch, H. P., Xavier, P. (2013). "A Drag Force Model to Incorporate the Reconfiguration of Full-Scale Riparian Trees Under Hydrodynamic Loading." J. Hydraul. Res., 51(5), 569-580.
Whittaker, P. (2014). "Modelling the Hydrodynamic Drag Force of Flexible Riparian Woodland." Doctoral Thesis, Hydro-Environmental Research Centre, Cardiff University, United Kingdom, p. 191.
Whittaker, P., Wilson, C.A.M.E., Aberle, J. (2015). An improved Cauchy number approach for predicting the drag and reconfiguration of flexible vegetation, Advances in Water Resources, 83, 28-35.
Wilson, C. A. M. E., and Horritt, M. S. (2002). "Measuring the Flow Resistance of Submerged Grass." Hydrol. Process., 16(13), 2589-2598.
Wilson, C. A. M. E., Yagci, O., Rauch, H., Stoesser, T. (2006). "Application of the Drag Force Approach to Model the Flow-Interaction of Natural Vegetation." Intl. J. River Basin Manag., 4(2), 137-146.
Wilson, C. A. M. E., Hoyt, J., Schnauder, I. (2008). "Impact of Foliage on the Drag Force of Vegetation in Aquatic Flows." J. Hydraul. Eng., 134(7), 885-891.
Wilson, C. A. M. E., Xavier, P., Schoneboom, T., Aberle, J., Rauch, H.-P., Lammeranner, W., Weissteiner, C., Thomas, H. (2010). "The hydrodynamic drag of full scale trees." Proc., Int. Conf. River Flow 2010, Bundensanstalt für Wasserbau, Karlsruhe, Braunschweig, Germany, 453-459.

Xavier, P. (2009). Floodplain Woodland Hydrodynamics, PhD thesis Ed., Hydro-environmental Research Centre, Cardiff University, Cardiff, United Kingdom, p. 510.
Yen, B. (2002). "Open Channel Flow Resistance." J. Hydraul. Eng., 128(1), 20-39.
Zinke, P., Olsen, N. R. B., Sukhodolova, T. (2008). "Modelling of hydraulics and morphodynamics in a vegetated river reach." Taylor & Francis, Cesme/Izmir, Turkey, 367-376.
Zinke, P. (2011). "Modelling of Flow and Levee Depositions in a Freshwater Delta with Natural Vegetation." PhD thesis, Norwegian University of Science and Technology, Faculty of Civil Engineering, p. 309.
Zinke, P. (2013). "Elasticity measurements for selected north european floodplain species." Proc., 35th IAHR World Congress, Tsinghua University Press., Chengdu, China, p. 10.

Aalto-DD 137/2015

ISBN 978-952-60-6384-3 (printed)
ISBN 978-952-60-6385-0 (pdf)
ISSN-L 1799-4934
ISSN 1799-4934 (printed)
ISSN 1799-4942 (pdf)

**Aalto University**
**School of Engineering**
**Department of Civil and Environmental Engineering**
**www.aalto.fi**

**BUSINESS + ECONOMY**

**ART + DESIGN + ARCHITECTURE**

**SCIENCE + TECHNOLOGY**

**CROSSOVER**

**DOCTORAL DISSERTATIONS**